Hamiltonian effective field theory in elongated or moving finite volume

Yan Li,[1,*] Jia-Jun Wu,[1,†] Derek B. Leinweber,[2] and Anthony W. Thomas[2,3]

[1]*School of Physical Sciences, University of Chinese Academy of Sciences (UCAS), Beijing 100049, China*
[2]*Special Research Centre for the Subatomic Structure of Matter (CSSM), Department of Physics, University of Adelaide, Adelaide, South Australia 5005, Australia*
[3]*ARC Centre of Excellence for Particle Physics at the Terascale (CoEPP), Department of Physics, University of Adelaide, Adelaide, South Australia 5005, Australia*

(Received 23 March 2021; accepted 20 April 2021; published 24 May 2021)

We extend previous work concerning rest-frame partial-wave mixing in Hamiltonian effective field theory to both elongated and moving systems, where two particles are in a periodic elongated cube or have nonzero total momentum, respectively. We also consider the combination of the two systems when directions of the elongation and the moving momentum are aligned. This extension should also be applicable in any Hamiltonian formalism. As a demonstration, we analyze lattice QCD results for the spectrum of an isospin-2 $\pi\pi$ scattering system and determine the s, d, and g partial-wave scattering information. The inclusion of lattice simulation results from moving frames significantly improves the uncertainty in the scattering information.

DOI: 10.1103/PhysRevD.103.094518

I. INTRODUCTION

Lattice simulations of relativistic quantum-field theories are performed in a Euclidean four-dimensional finite volume. Scattering states are contained in the finite box with discretized energy levels. Understanding the relationship between these finite-volume energy levels and experimental scattering observables such as the phase shift and inelasticity is of significance. For the case of elastic two-body scattering in the rest frame, Lüscher [1–3] found a model-independent formula which is now known as Lüscher's formula.

An equivalent approach is provided in Hamiltonian effective field theory (HEFT) [4–12], a Hamiltonian extension of chiral effective field theory. In the standard approach, a Hamiltonian which respects the constraints of chiral effective field theory is fit to the finite-volume energy spectrum of lattice field theory and the infinite-volume scattering observables are obtained from the constrained Hamiltonian. The approach bridges finite-volume lattice field theory and experimental observables while providing insight into the composition of the scattering states in terms of noninteracting multiparticle basis states.

Different partial waves are mixed in the finite volume as a result of broken spherical symmetry. This mixing complicates the construction of the Hamiltonian matrix. For example, its incorporation significantly increases the dimension of the matrix. A recent work [12] established a formalism for disentangling partial-wave mixing and maximally reducing the dimension of the Hamiltonian matrix in the finite volume via an optimal set of rest-frame basis states. In this work, we will generalize this formalism to both elongated and moving systems with nontrivial total momentum. We will also consider the combination of these two systems when the direction of elongation and that of the moving momentum are aligned.

The Lüscher formula has already been extended and applied to the case of rectangular cuboid boxes [13–23]. This work will first consider a more general case where the box is allowed to be a general parallelepiped, as illustrated in Fig. 1. We then focus on a special class of the parallelepiped termed an elongated cube.

The Lüscher formula has also been extended to moving systems [25–30]. To realize the extension in a Hamiltonian formalism, one needs a Hamiltonian making contact with both the infinite-volume scattering observables parametrized in the rest frame and the finite-volume spectrum in the moving frame. This can be achieved within the formalism proposed in Refs. [31,32]. In that formalism, different forms of the moving-frame Lüscher formula are unified as different momentum transformations. Furthermore it leads to a new momentum transformation which is not only useful in the Hamiltonian formalism, but can also be used in the finite-volume three-particle quantization condition [33].

*liyan175@mails.ucas.edu.cn
†wujiajun@ucas.ac.cn

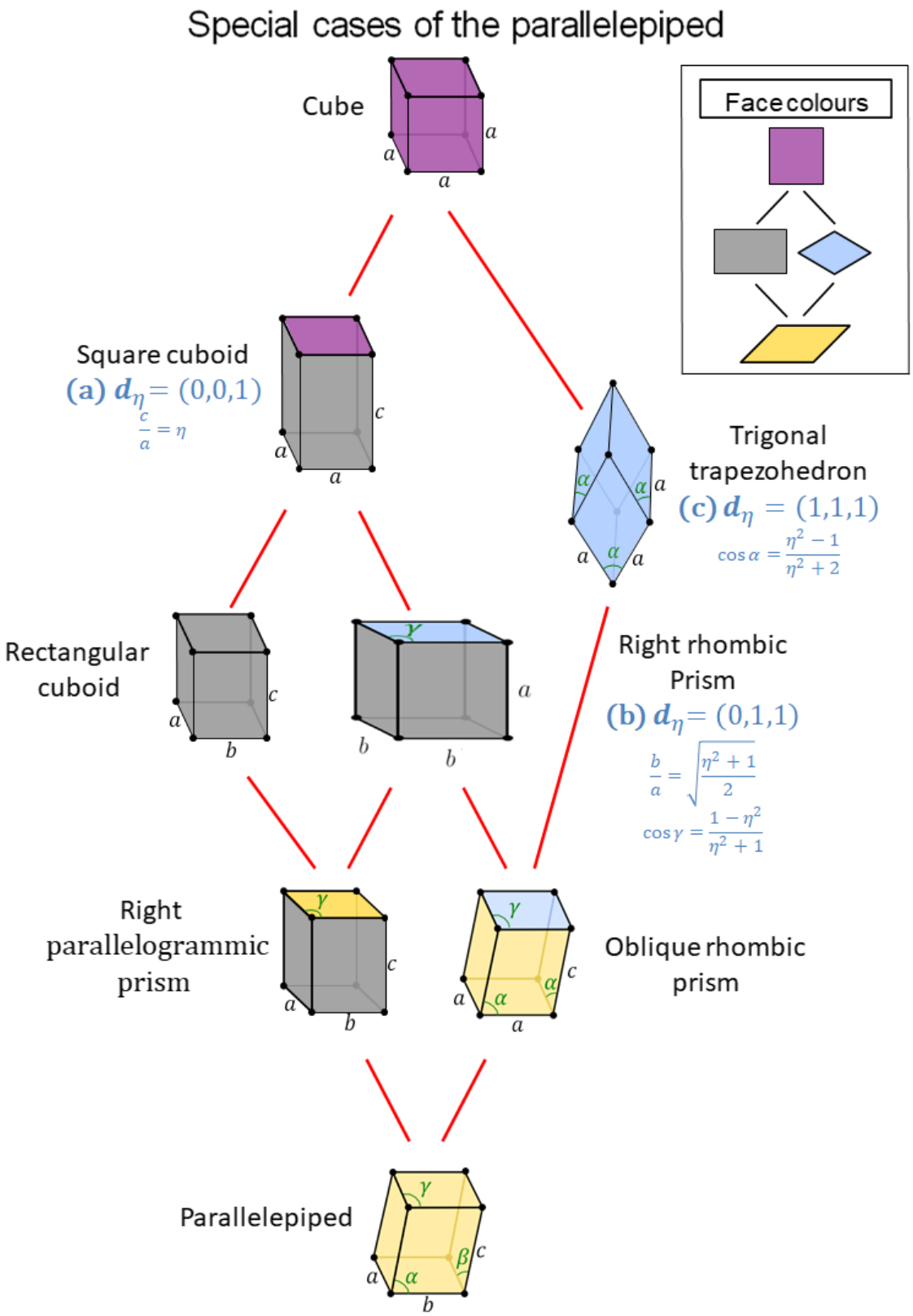

FIG. 1. Special cases of the parallelepiped (taken from Ref. [24] with slight modifications). The elongated cubes discussed in this work are labeled with the elongated vector $\mathbf{d}_\eta$.

The symmetry in a moving frame is quite compatible with a cube elongated in the same direction as the nonzero total momentum. This case will be termed the elongated moving system, and disentangling partial-wave mixing in the elongated moving system is the main concern of this work. We will also demonstrate how the formalism works by analyzing lattice QCD results from Ref. [34] for the spectrum of an isospin-2 $\pi\pi$ scattering system. As also noted in Ref. [12], the discussion in this work should apply not only in HEFT, but also in any Hamiltonian formalism, e.g., the harmonic oscillator basis effective theory [35–37].

There are also many other extensions of the Lüscher formula, including the multichannel case [38–43], nonzero spins [44–47], twisted-boundary conditions [48–51] and the multibody case [33,52–71]. With the exception of the many-body case, these extensions should be easily realized in the Hamiltonian formalism using the results of Ref. [12] and this paper. In addition, there have also been studies concerning finite-spacing effects in the Hamiltonian formalism, e.g., Ref. [72].

This paper is organized as follows. In Sec. II, the finite-volume Hamiltonian in the elongated moving system is established. Section III accommodates partial-wave mixing in the elongated moving system using the formalism developed in Ref. [12]. Section IV demonstrates how this formalism works by analyzing lattice QCD results for isospin-2 $\pi\pi$ scattering [34]. Finally, the results are summarized in Sec. V.

II. HAMILTONIAN IN ELONGATED MOVING FINITE VOLUME

A. Parallelepiped and elongated cube

Normally, the system under consideration in lattice field theory simulations is a periodic cube. However, there are good reasons to also consider asymmetric boxes, where longer dimensions provide access to smaller nontrivial momenta [73]. For example, Ref. [13] studied a rectangular cuboid (including the square cuboid as a special case). In general, the box can be a parallelepiped as shown in Fig. 1.

If we choose one of the vertices of the parallelepiped as the origin, the parallelepiped can be specified by the three vectors $\mathbf{a}$, $\mathbf{b}$, $\mathbf{c}$ corresponding to the edges connected to the origin. The three vectors specify a matrix

$$M = \begin{bmatrix} a_1 & b_1 & c_1 \\ a_2 & b_2 & c_2 \\ a_3 & b_3 & c_3 \end{bmatrix}, \tag{1}$$

which sends the three unit vectors of the coordinate axes to $\mathbf{a}$, $\mathbf{b}$, and $\mathbf{c}$ respectively, where the subscripts denote the coordinate components of the vectors. To restrict the range of $\mathbf{x}^*$ within the parallelepiped, one can define $\mathbf{x}^*$ via $x_i^* = \sum_j M_{ij} x_j$ and constrain $\mathbf{x}$ within the unit cube. Correspondingly, when imposing the periodic boundary condition, the momentum $\mathbf{k}^*$ should be discretized as

$$k_i^* = \sum_j M_{ij}^{-1} \frac{2\pi}{L} n_j, \qquad n_j \in \mathbb{Z}, \tag{2}$$

where we replace the unit cube with a cube of edge length L, as is standard in lattice field theory.

Here, we do not consider all the cases in Fig. 1 since in most cases the symmetries are broken too much. When we study moving frames in the following sections, we will find that the symmetry of a cube elongated in the same direction as the moving momentum is quite compatible with the moving effects. So in this paper, we define the elongated cube as a cube elongated in a specific direction $\hat{\mathbf{d}}_\eta$ with a magnitude η, and we consider three $\mathbf{d}_\eta$ as follows:

(a)

$$\mathbf{d}_\eta = (0,0,1), \qquad M = \begin{bmatrix} 1 & & \\ & 1 & \\ & & \eta \end{bmatrix},$$

corresponding to the square cuboid (already covered in Ref. [13]), labeled as (a) in Fig. 1.

(b)

$$\mathbf{d}_\eta = (0,1,1), \qquad M = \begin{bmatrix} 1 & 0 & 0 \\ 0 & \frac{\eta+1}{2} & \frac{\eta-1}{2} \\ 0 & \frac{\eta-1}{2} & \frac{\eta+1}{2} \end{bmatrix},$$

corresponding to the right rhombic prism, labeled as (b) in Fig. 1. We note that not all right rhombic prisms are included in this scenario, since $\frac{b}{a} = \sqrt{\frac{\eta^2+1}{2}}$ and $\cos\gamma = \frac{1-\eta^2}{\eta^2+1}$ are both determined by η. The general right rhombic prism corresponds to

$$M = \begin{bmatrix} \eta_x & 0 & 0 \\ 0 & \frac{\eta+1}{2} & \frac{\eta-1}{2} \\ 0 & \frac{\eta-1}{2} & \frac{\eta+1}{2} \end{bmatrix},$$

which is an elongated cube only when $\eta_x = 1$.

(c)

$$\mathbf{d}_\eta = (1,1,1), \qquad M = \begin{bmatrix} \frac{\eta+2}{3} & \frac{\eta-1}{3} & \frac{\eta-1}{3} \\ \frac{\eta-1}{3} & \frac{\eta+2}{3} & \frac{\eta-1}{3} \\ \frac{\eta-1}{3} & \frac{\eta-1}{3} & \frac{\eta+2}{3} \end{bmatrix},$$

corresponding to the trigonal trapezohedron, labeled as (c) in Fig. 1.

We note that the overall factors of $\mathbf{d}_\eta$ are not important, and are taken as presented for further convenience. In the elongated cube, the momentum is discretized as

$$\mathbf{k}^* = \frac{2\pi}{L}\left(\mathbf{n}_\perp + \frac{1}{\eta}\mathbf{n}_\parallel\right), \qquad \mathbf{n} \in \mathbb{Z}^3, \tag{3}$$

where the $\perp$ and $\parallel$ components of a vector are defined through

$$\mathbf{n}_\parallel \coloneqq \frac{\mathbf{n}\cdot\mathbf{d}_\eta}{|\mathbf{d}_\eta|^2}\mathbf{d}_\eta, \qquad \mathbf{n}_\perp \coloneqq \mathbf{n} - \mathbf{n}_\parallel. \tag{4}$$

To be more concrete, for an infinite-volume Hamiltonian

$$H = \int \frac{d^3\mathbf{k}^*}{(2\pi)^3} h(k^*)|\mathbf{k}^*\rangle\langle\mathbf{k}^*| + \int \frac{d^3\mathbf{k}'^*}{(2\pi)^3}\frac{d^3\mathbf{k}^*}{(2\pi)^3} V(\mathbf{k}'^*, \mathbf{k}^*)|\mathbf{k}'^*\rangle\langle\mathbf{k}^*|, \tag{5}$$

where h and V denote the kinetic and potential energy respectively, and the state $|\mathbf{k}^*\rangle$ is normalized as

$$\langle\mathbf{k}'^*|\mathbf{k}^*\rangle = (2\pi)^3\delta^3(\mathbf{k}'^* - \mathbf{k}^*), \tag{6}$$

to put it in an elongated cube, we need the discretization

$$\int \frac{d^3\mathbf{k}^*}{(2\pi)^3} \to \eta^{-1}L^{-3}\sum_{\mathbf{k}^*=\frac{2\pi}{L}(\mathbf{n}_\perp+\frac{1}{\eta}\mathbf{n}_\parallel),\mathbf{n}\in\mathbb{Z}^3}, \tag{7}$$

and

$$|\mathbf{k}^*\rangle \to \eta^{\frac{1}{2}}L^{\frac{3}{2}}|\mathbf{n}\rangle \tag{8}$$

so that the basis $|\mathbf{n}\rangle$ is orthonormal

$$\langle\mathbf{n}'|\mathbf{n}\rangle = \delta_{\mathbf{n}'\mathbf{n}}. \tag{9}$$

Finally, the Hamiltonian in a finite elongated cube is

$$H_L = \sum_{\mathbf{n}} h(k^*(\mathbf{n}))|\mathbf{n}\rangle\langle\mathbf{n}| + \sum_{\mathbf{n}',\mathbf{n}} \eta^{-1}L^{-3}V(\mathbf{k}^*(\mathbf{n}'), \mathbf{k}^*(\mathbf{n}))|\mathbf{n}'\rangle\langle\mathbf{n}|. \tag{10}$$

We note the Hamiltonian Eq. (10) applies to any elongated cubes, including those of the three scenarios (a), (b) and (c) introduced above Eq. (3).

We also note that the box studied in Ref. [13] corresponds to

$$M = \begin{bmatrix} \eta_1 & & \\ & \eta_2 & \\ & & \eta_3 \end{bmatrix}, \tag{11}$$

where an overall factor can be absorbed into L. This box corresponds to the rectangular cuboid, which is not completely equivalent to the elongated cube, since it needs elongation in more than one direction. However in some cases, $\eta_1 = \eta_2 = 1$ for instance, the box is an elongated cube with $\mathbf{d}_\eta = (0, 0, 1)$.

B. Moving system

Since the infinite-volume potential and scattering observables are most easily parametrized in the rest frame, we need a Hamiltonian that can produce the moving-frame spectrum while still written in terms of the rest-frame potential.

As suggested in Refs. [31,32], one can introduce a momentum transformation $\mathbf{k}^* \to \mathbf{k}$ to the infinite-volume Hamiltonian

$$\begin{aligned} H &= \int \frac{d^3\mathbf{k}^*}{(2\pi)^3} h(k^*)|\mathbf{k}^*\rangle\langle\mathbf{k}^*| + \int \frac{d^3\mathbf{k}'^*}{(2\pi)^3}\frac{d^3\mathbf{k}^*}{(2\pi)^3} V(\mathbf{k}'^*, \mathbf{k}^*)|\mathbf{k}'^*\rangle\langle\mathbf{k}^*| \\ &= \int \frac{d^3\mathbf{k}}{(2\pi)^3}\mathcal{J}(\mathbf{k})h(k^*(\mathbf{k}))|\mathbf{k}^*(\mathbf{k})\rangle\langle\mathbf{k}^*(\mathbf{k})| \\ &\quad + \int \frac{d^3\mathbf{k}'}{(2\pi)^3}\mathcal{J}(\mathbf{k}')\frac{d^3\mathbf{k}}{(2\pi)^3}\mathcal{J}(\mathbf{k})V(\mathbf{k}^*(\mathbf{k}'), \mathbf{k}^*(\mathbf{k})) \\ &\quad \times |\mathbf{k}^*(\mathbf{k}')\rangle\langle\mathbf{k}^*(\mathbf{k})|, \end{aligned} \tag{12}$$

where $\mathcal{J}$ denotes the Jacobian of the transformation. Then one can define

$$|\mathbf{k}\rangle \coloneqq \mathcal{J}^{\frac{1}{2}}(\mathbf{k})|\mathbf{k}^*(\mathbf{k})\rangle, \tag{13}$$

such that

$$\langle\mathbf{k}'|\mathbf{k}\rangle = \mathcal{J}(\mathbf{k})(2\pi)^3\delta^3(\mathbf{k}'^* - \mathbf{k}^*) = (2\pi)^3\delta^3(\mathbf{k}' - \mathbf{k}), \tag{14}$$

and the infinite-volume Hamiltonian will be

$$H = \int \frac{d^3\mathbf{k}}{(2\pi)^3} h(k^*(\mathbf{k}))|\mathbf{k}\rangle\langle\mathbf{k}| + \int \frac{d^3\mathbf{k}'}{(2\pi)^3}\frac{d^3\mathbf{k}}{(2\pi)^3}[\mathcal{J}^{\frac{1}{2}}(\mathbf{k}')V(\mathbf{k}^*(\mathbf{k}'), \mathbf{k}^*(\mathbf{k}))\mathcal{J}^{\frac{1}{2}}(\mathbf{k})]|\mathbf{k}'\rangle\langle\mathbf{k}|. \tag{15}$$

Now if one discretizes $\mathbf{k}$ instead of $\mathbf{k}^*$, one gets a different finite-volume Hamiltonian

$$H_L = \sum_{\mathbf{n}} h(k^*(\mathbf{n}))|\mathbf{n}\rangle\langle\mathbf{n}| + \sum_{\mathbf{n}',\mathbf{n}} L^{-3}\tilde{V}(\mathbf{k}(\mathbf{n}'), \mathbf{k}(\mathbf{n}))|\mathbf{n}'\rangle\langle\mathbf{n}|$$

$$\tilde{V}(\mathbf{k}', \mathbf{k}) = [\mathcal{J}^{\frac{1}{2}}(\mathbf{k}')V(\mathbf{k}'^*, \mathbf{k}^*)\mathcal{J}^{\frac{1}{2}}(\mathbf{k})], \qquad \mathbf{k} = \frac{2\pi}{L}\mathbf{n}. \tag{16}$$

Reference [31] proposed a number of general momentum transformations for the moving system, and proved that those transformations can keep the relationship between the infinite-volume phase shifts and finite-volume spectrum up to exponentially suppressed corrections. That paper also studied three typical transformations. While two of the three have been used in many previous works [25–27], they introduce additional energy dependence. The third one (labeled as scheme C in Ref. [31]) does not have such problems and hence is suitable here. It reads

$$\mathbf{k}^* = \mathbf{k}_\perp + \gamma\left(\mathbf{k}_\parallel - \frac{\omega_1(\mathbf{k})}{\omega_1(\mathbf{k})+\omega_2(\mathbf{P}-\mathbf{k})}\mathbf{P}\right),$$
$$\gamma = \frac{\omega_1(\mathbf{k})+\omega_2(\mathbf{P}-\mathbf{k})}{\sqrt{(\omega_1(\mathbf{k})+\omega_2(\mathbf{P}-\mathbf{k}))^2-\mathbf{P}^2}}, \tag{17}$$

where $\omega_i(\mathbf{k}) = \sqrt{k^2+m_i^2}$ and $\mathbf{P}$ is the total momentum of the moving system, and the corresponding Jacobian is

$$\mathcal{J}(\mathbf{k}) = \frac{\omega_1(\mathbf{k})+\omega_2(\mathbf{P}-\mathbf{k})}{\omega_1(\mathbf{k})\omega_2(\mathbf{P}-\mathbf{k})} \Big/ \frac{\omega_1(\mathbf{k}^*)+\omega_2(\mathbf{k}^*)}{\omega_1(\mathbf{k}^*)\omega_2(\mathbf{k}^*)}. \tag{18}$$

In the finite cube, the total momentum can only take discrete values as $\mathbf{P} = \frac{2\pi}{L}\mathbf{d}_\gamma$ with $\mathbf{d}_\gamma$ an integer vector.

C. Elongated moving system

Both the elongated and moving systems have smaller finite-volume symmetry groups than the rest-frame cube, and combining them will normally give a much smaller one. However, if the elongated direction and the moving direction are the same, their combination will not see a large reduction in symmetry. We will call this combination the elongated moving system. The corresponding finite-volume Hamiltonian is obtained by combining Eqs. (10) and (16), which reads

$$H_L = \sum_{\mathbf{n}} h(k^*(\mathbf{n}))|\mathbf{n}\rangle\langle\mathbf{n}| + \sum_{\mathbf{n}',\mathbf{n}} \eta^{-1}L^{-3}\tilde{V}(\mathbf{k}(\mathbf{n}'),\mathbf{k}(\mathbf{n}))|\mathbf{n}'\rangle\langle\mathbf{n}|$$
$$\tilde{V}(\mathbf{k}',\mathbf{k}) = \mathcal{J}^{\frac{1}{2}}(\mathbf{k}')V(\mathbf{k}'^*,\mathbf{k}^*)\mathcal{J}^{\frac{1}{2}}(\mathbf{k}),$$
$$\mathbf{k} = \frac{2\pi}{L}\left(\mathbf{n}_\perp + \frac{1}{\eta}\mathbf{n}_\parallel\right), \tag{19}$$

where the momentum transformation $\mathbf{k}^* \to \mathbf{k}$ and the corresponding Jacobian is the same as Eqs. (17) and (18) for the moving system, except that the total momentum $\mathbf{P}$ should now be

$$\mathbf{P} = \frac{1}{\eta}\frac{2\pi}{L}\mathbf{d}_\gamma, \tag{20}$$

noting either $\mathbf{d}_\eta = \mathbf{d}_\gamma$ or $\eta = 1$ for $\mathbf{P} \neq \mathbf{0}$ in this "elongated moving system."

Now Eqs. (17)–(20) are all the ingredients needed to write down the elongated moving Hamiltonian. The eigenvalues of this Hamiltonian are rest-frame energies E_n^* related to moving-frame energies E_n via

$$E_n = \sqrt{E_n^{*2}+\mathbf{P}^2}. \tag{21}$$

Since the kinetic energy $h(k^*)$ depends only on the length of $\mathbf{k}^*$, one can separate the kinetic term as

$$\sum_{\mathbf{n}} h(k^*)|\mathbf{n}\rangle\langle\mathbf{n}| = \sum_{e_n} h(k^*)\sum_{\hat{e}_n}|\mathbf{n}\rangle\langle\mathbf{n}|, \tag{22}$$

so that k^* depends only on e_n (and $\sum_{\hat{e}_n}$ is simply defined to sum over all the $\mathbf{n}$ with the same e_n). In other words, e_n denotes a degenerate shell of the basis-state Hamiltonian, H_0, describing the energies of the noninteracting states. Note, there can be several values for e_n related to vectors $\mathbf{n}$, $\mathbf{d}_\eta$ and $\mathbf{d}_\gamma$ all providing the same degenerate value for $h(k^*)$.

It is interesting to consider how the elongated moving system reduces to more simple cases for certain values of $\mathbf{d}_\eta$, η and $\mathbf{d}_\gamma$. When the masses of the two particles are the same, we also have

$$\mathbf{n} \to \mathbf{d}_\gamma - \mathbf{n} \Rightarrow \mathbf{k}^* \to -\mathbf{k}^* \Rightarrow h(k^*) \text{ invariant}. \tag{23}$$

Thus our discussion for the degenerate shells splits into four cases as listed in Table I. There we introduce an elongated moving vector $\mathbf{d} \neq \mathbf{0}$, since either we can set $\mathbf{d}_\eta = \mathbf{d}_\gamma$ or choose one of the two vectors to vanish. In Table I, case A refers to the standard unelongated and rest-frame system. e_n can be simply chosen as $\mathbf{n}^2$. Case B refers to the elongated or unelongated moving-frame system with two particles of different mass. As suggested by Eq. (17), $h(k^*)$ now depends on $\mathbf{n}^2$, $(\mathbf{d}-\mathbf{n})^2$, $\mathbf{n}_\parallel^2$, and $\mathbf{n}_\perp^2$. Because both $\mathbf{n}_\parallel^2$ and $\mathbf{n}_\perp^2$ can be reexpressed in terms of $\mathbf{n}^2$ and $(\mathbf{d}-\mathbf{n})^2$, e_n can be chosen as $(\mathbf{n}^2,(\mathbf{d}-\mathbf{n})^2)$, or $(\mathbf{n}^2,\mathbf{n}\cdot\mathbf{d})$ equivalently. Case C1 refers to the elongated rest-frame system. $h(k^*)$ now depends on $\mathbf{n}^2$, $\mathbf{n}_\parallel^2 \propto |\mathbf{n}\cdot\mathbf{d}|^2$, and $\mathbf{n}_\perp^2 = \mathbf{n}^2 - \mathbf{n}_\parallel^2$. Thus e_n can be chosen as $(\mathbf{n}^2,|\mathbf{n}\cdot\mathbf{d}|)$. Case C2 refers to the elongated or unelongated moving-

TABLE I. Four different cases for the degenerate shells. The $\{\mathbf{n}^2,(\mathbf{d}-\mathbf{n})^2\}$ in the C2 row is an unordered pair.

Case	$\mathbf{d}_\eta$	η	$\mathbf{d}_\gamma$	$m_1 = m_2$?	e_n
A	any	$=1$	0	Any	$\mathbf{n}^2$
B	$\mathbf{d}\neq\mathbf{0}$	Any	$\mathbf{d}\neq\mathbf{0}$	No	$(\mathbf{n}^2,(\mathbf{d}-\mathbf{n})^2)$ or $(\mathbf{n}^2,\mathbf{n}\cdot\mathbf{d})$
C1	$\mathbf{d}\neq\mathbf{0}$	$\neq 1$	0	Any	$(\mathbf{n}^2,\lvert\mathbf{n}\cdot\mathbf{d}\rvert)$
C2	$\mathbf{d}\neq\mathbf{0}$	Any	$\mathbf{d}\neq\mathbf{0}$	Yes	$\{\mathbf{n}^2,(\mathbf{d}-\mathbf{n})^2\}$

frame system with two particles of the same mass. In contrast to case B, $\mathbf{n}$ and $\mathbf{d}-\mathbf{n}$ are on the same shell as indicated by Eq. (23). As $(\mathbf{n}^2, (\mathbf{d}-\mathbf{n})^2)$ and $((\mathbf{d}-\mathbf{n})^2, \mathbf{n}^2)$ denote the same shell, e_n can be chosen as an unordered pair $\{\mathbf{n}^2, (\mathbf{d}-\mathbf{n})^2\}$.

III. PARTIAL-WAVE MIXING IN AN ELONGATED MOVING SYSTEM

Spherical symmetry allows the following partial-wave expansion:

$$V(\mathbf{k}'^*, \mathbf{k}^*) = \sum_l v_l(k'^*, k^*) \sum_m Y_{lm}(\hat{\mathbf{k}}'^*) Y^*_{lm}(\hat{\mathbf{k}}^*), \quad (24)$$

where $Y_{lm}(\hat{\mathbf{k}}^*)$ are the usual spherical harmonics, as shown in Eq. (B1), and its variables are the direction angles (θ^*, ϕ^*) of the vector $\mathbf{k}^*$. Different partial waves are decoupled under this potential in the infinite volume. In the finite volume, partial wave numbers (l, m) are no longer good quantum numbers, and the partial wave potentials v_l with different l are coupled together in the determination of finite-volume spectra. This phenomena, called partial-wave mixing, complicates the structure of the Hamiltonian Eq. (19). In the standard case (case A in Table I), Ref. [12] proposed a method that provides an optimal set of basis states maximally reducing the dimension of the Hamiltonian. In this section, we will generalize that method to more general cases.

The spherical symmetry group SO(3) is broken into one of its subgroups G in the finite volume. In the standard case A, G is the octahedral group O. In other cases in Table I, G is smaller, and turns out to be also a subgroup of a two-dimensional rotation group O(2) [or $\mathrm{O}(2) \times \mathrm{C}_2$ in case C], where the rotation axis of this O(2) should be the same as the elongated moving vector $\mathbf{d}$. This prefers the partial wave expansion Eq. (24) expanded in a coordinate system different from that of the discretized momentum. Appendix A discusses how the coordinate system is chosen (results are summarized in Table XIV).

In general cases, we expect the finite-volume potential in Eq. (19) can be put in a similar form as Eq. (24) as follows:

$$\tilde{V}(\mathbf{k}', \mathbf{k}) = \sum_{\Gamma_\infty} \tilde{v}_{\Gamma_\infty}(e'_n, e_n) \sum_{\alpha_\infty} u_{\Gamma_\infty,\alpha_\infty}(\mathbf{n}') u^*_{\Gamma_\infty,\alpha_\infty}(\mathbf{n}), \quad (25)$$

where α_∞ denotes the index of the vector of the irreducible representation Γ_∞ of the group G_∞, and the definitions for $u_{\Gamma_\infty,\alpha_\infty}$ and $\tilde{v}_{\Gamma_\infty}$ are summarized in Table II. In the Table, we also have

$$S_m = \begin{cases} + & m \geq 0 \\ - & m < 0 \end{cases}, \qquad \sum_{l^\mathcal{P}} = \begin{cases} \text{sum over evens} & \mathcal{P} = + \\ \text{sum over odds} & \mathcal{P} = - \end{cases}, \quad (26)$$

and $S^\mathcal{P}(m, \theta^*)$ is defined via

$$P_{lm}(\cos\theta^*) = \begin{cases} S^+(m,\theta^*) P_{lm}(|\cos\theta^*|) & l \text{ is even} \\ S^-(m,\theta^*) P_{lm}(|\cos\theta^*|) & l \text{ is odd,} \end{cases} \quad (27)$$

which gives

$$S^+(m,\theta^*) = \begin{cases} +1 & \cos\theta^* \geq 0 \\ (-1)^m & \cos\theta^* < 0, \end{cases}$$
$$S^-(m,\theta^*) = \begin{cases} +1 & \cos\theta^* \geq 0 \\ (-1)^{m+1} & \cos\theta^* < 0. \end{cases} \quad (28)$$

In the standard case, Eq. (25) becomes the same as Eq. (24). In case B, we now take O(2) as G_∞, and the α_∞-independence of $\tilde{v}_{\Gamma_\infty}$ comes from the invariance of

$$\frac{(l-m)!}{(l+m)!} P_{lm}(\cos\theta'^*) P_{lm}(\cos\theta^*) \quad (29)$$

under $m \to -m$. In case C, G_∞ is now $\mathrm{O}(2) \times \mathrm{C}_2$, where the C_2 symmetry comes from $\mathbf{k} \to \mathbf{P} - \mathbf{k}$, i.e., exchanging the momenta of the two equal-mass particles, and is different from the parity symmetry in the usual sense. In the latter case, one is concerned with $\mathbf{k} \to -\mathbf{k}$ and $\mathbf{P} \to -\mathbf{P}$. It is now $|\cos\theta^*|$ instead of $\cos\theta^*$ independent of $\hat{e}_n$.

In what follows, we will show how to construct the optimal set of basis states maximally reducing the dimension of the finite-volume Hamiltonian in general cases. The formalism is basically the same as that in Ref. [12], except with a different language introduced above.

TABLE II. Some definitions for different cases. α_∞ denotes the index of the vector of the irreducible representation Γ_∞ of the group G_∞.

Case	A	B	C1 or C2
G_∞	O(3)	O(2)	$\mathrm{O}(2) \times \mathrm{C}_2$
$(\Gamma_\infty, \alpha_\infty)$	$(l^\mathcal{P}, m)$	$(\lvert m\rvert, S_m)$	$(\lvert m\rvert^\mathcal{P}, S_m)$
$\tilde{v}_{\Gamma_\infty}$	v_l	$\mathcal{J}^{\frac{1}{2}}(\mathbf{k}')\mathcal{J}^{\frac{1}{2}}(\mathbf{k}) \sum_l v_l \frac{2l+1}{4\pi}\frac{(l-m)!}{(l+m)!} \times P_{lm}(\cos\theta'^*) P_{lm}(\cos\theta^*)$	$\mathcal{J}^{\frac{1}{2}}(\mathbf{k}')\mathcal{J}^{\frac{1}{2}}(\mathbf{k}) \sum_{l^\mathcal{P}} v_l \frac{2l+1}{4\pi}\frac{(l-m)!}{(l+m)!} \times P_{lm}(\lvert\cos\theta'^*\rvert) P_{lm}(\lvert\cos\theta^*\rvert)$
$u_{\Gamma_\infty,\alpha_\infty}$	Y_{lm}	$e^{im\phi^*}$	$S^\mathcal{P}(m,\theta^*) e^{im\phi^*}$

Now one can introduce

$$|e_n;\Gamma_\infty,\alpha_\infty\rangle = \sum_{\hat{e}_n} u_{\Gamma_\infty,\alpha_\infty}(\mathbf{n})|\mathbf{n}\rangle \tag{30}$$

to write V_L as

$$V_L = \eta^{-1}L^{-3}\sum_{e_n',e_n;\Gamma_\infty}\tilde{v}_{\Gamma_\infty}(e_n',e_n)\sum_{\alpha_\infty}|e_n';\Gamma_\infty,\alpha_\infty\rangle\langle e_n;\Gamma_\infty,\alpha_\infty|, \tag{31}$$

and construct the states $|e_n,\Gamma_\infty;\Gamma,f,\alpha\rangle$ via linear combinations of $|e_n;\Gamma_\infty,\alpha_\infty\rangle$ as follows:

$$|e_n,\Gamma_\infty;\Gamma,f,\alpha\rangle = \sum_{\alpha_\infty}[C_{\Gamma_\infty}]_{\alpha_\infty;\Gamma,f,\alpha}|e_n;\Gamma_\infty,\alpha_\infty\rangle, \tag{32}$$

where Γ, f and α denote the αth vector of the fth occurrence of the irreducible representation Γ reduced from the Γ_∞, and the coefficients derived from group theory can be found in Appendix A.

One can then define the inner product matrices for these states as

$$[P_{e_n}]_{\Gamma_\infty',\alpha_\infty';\Gamma_\infty,\alpha_\infty} \coloneqq \langle e_n;\Gamma_\infty',\alpha_\infty'|e_n;\Gamma_\infty,\alpha_\infty\rangle, \tag{33}$$

and

$$\begin{aligned}&[P_{e_n;\Gamma,\alpha}]_{\Gamma_\infty',f';\Gamma_\infty,f}\\ &\quad\coloneqq \langle e_n,\Gamma_\infty';\Gamma,f',\alpha|e_n,\Gamma_\infty;\Gamma,f,\alpha\rangle\\ &\quad= \sum_{\alpha_\infty',\alpha_\infty}[C_{\Gamma_\infty'}]^*_{\alpha_\infty';\Gamma,f',\alpha}[P_{e_n}]_{\Gamma_\infty',\alpha_\infty';\Gamma_\infty,\alpha_\infty}[C_{\Gamma_\infty}]_{\alpha_\infty;\Gamma,f,\alpha}.\end{aligned} \tag{34}$$

Using these inner product matrices, one can orthonormalize $|e_n,\Gamma_\infty;\Gamma,f,\alpha\rangle$ to our final basis $|e_n;\Gamma,F,\alpha\rangle$. The Wigner-Eckart theorem only permits the following general form for the V_L:

$$\begin{aligned}V_L = \eta^{-1}L^{-3}&\sum_{e_n',e_n;\Gamma,F',F}\tilde{v}_{\Gamma,F',F}(e_n',e_n)\\ &\times\sum_{\alpha}|e_n';\Gamma,F',\alpha\rangle\langle e_n;\Gamma,F,\alpha|,\end{aligned} \tag{35}$$

which, combined with Eq. (31), leads to

$$\begin{aligned}&\tilde{v}_{\Gamma,F',F}(e_n',e_n) = \sum_{\Gamma_\infty}\tilde{v}_{\Gamma_\infty}(e_n',e_n)[G_{\Gamma_\infty,\Gamma}]_{e_n',F';e_n,F},\\ &[G_{\Gamma_\infty,\Gamma}]_{e_n',F';e_n,F} = \sum_f[M_{\Gamma_\infty;\Gamma,\alpha}]^*_{f;e_n',F'}[M_{\Gamma_\infty;\Gamma,\alpha}]_{f;e_n,F},\quad \forall\ \alpha,\\ &[M_{\Gamma_\infty;\Gamma,\alpha}]_{f;e_n,F} = \langle e_n,\Gamma_\infty;\Gamma,f,\alpha|e_n;\Gamma,F,\alpha\rangle.\end{aligned} \tag{36}$$

There are different methods to orthonormalize $|e_n,\Gamma_\infty;\Gamma,f,\alpha\rangle$. We present the result of the eigenmode-based method discussed in Ref. [12] as follows:

$$[M_{\Gamma_\infty;\Gamma,\alpha}]_{f;e_n,F} = \sqrt{\lambda^F}X^F_{\Gamma_\infty,f}, \tag{37}$$

where λ^F and $X^F_{\Gamma_\infty,f}$ are the Fth eigenvalue and the (Γ_∞,f)-component of the Fth eigenvector of the matrix $P_{e_n;\Gamma,\alpha}$ respectively.

IV. EXAMPLE OF ISOSPIN-2 $\pi\pi$ SCATTERING

In this section, following a similar discussion in Sec. IV of Ref. [12], we apply the formalism developed herein to analyze lattice QCD results for the isospin-2 $\pi\pi$ scattering system. This time, the moving-frame data is included in the analysis.

As in Ref. [12], the lattice QCD results are from Ref. [34] where an anisotropic action is used. They quote the anisotropy $\xi = a_s/a_t = 3.444(6)$ and the pion mass in lattice units $a_t m_\pi = 0.06906(13)$. The $\pi\pi$-channel is also studied in their other recent works [74–76]. Drawing on the scale setting provided in Ref. [76], $a_t^{-1} = 5.662$ GeV, m_π is approximately 391 MeV.

In the analysis performed in Ref. [34], lattice results above the 4π threshold were not included. Since our formalism does not include the four-body contributions, the same cut is employed.

A. The procedures

As in Ref. [12], we work with dimensionless lattice units. The kinetic energy h is taken as

$$a_t h(k) = 2\sqrt{(a_t m_\pi)^2 + (a_t k)^2}, \tag{38}$$

and when going to the finite-volume system, we have

$$a_t k \to a_t k_N = \frac{2\pi\sqrt{N}}{\xi L/a_s}, \tag{39}$$

where $N = \mathbf{n}^2$. Because the isospin is two, only s, d, and g waves need to be taken into account, as in Ref. [34]. With the partial-wave expansion of Eq. (24), the partial-wave potentials are taken to be of a simple separable form:

$$a_t^{-2}v_l(p,k) = \frac{G_l}{(a_t m_\pi)^2}f_l(p)f_l(k), \tag{40}$$

with

$$f_l(k) = \frac{(d_l a_t k)^l}{(1+(d_l a_t k)^2)^{l/2+2}}, \tag{41}$$

with parameters G_l and d_l dimensionless.

The parameters in these potentials were fit to minimize the χ^2 defined by

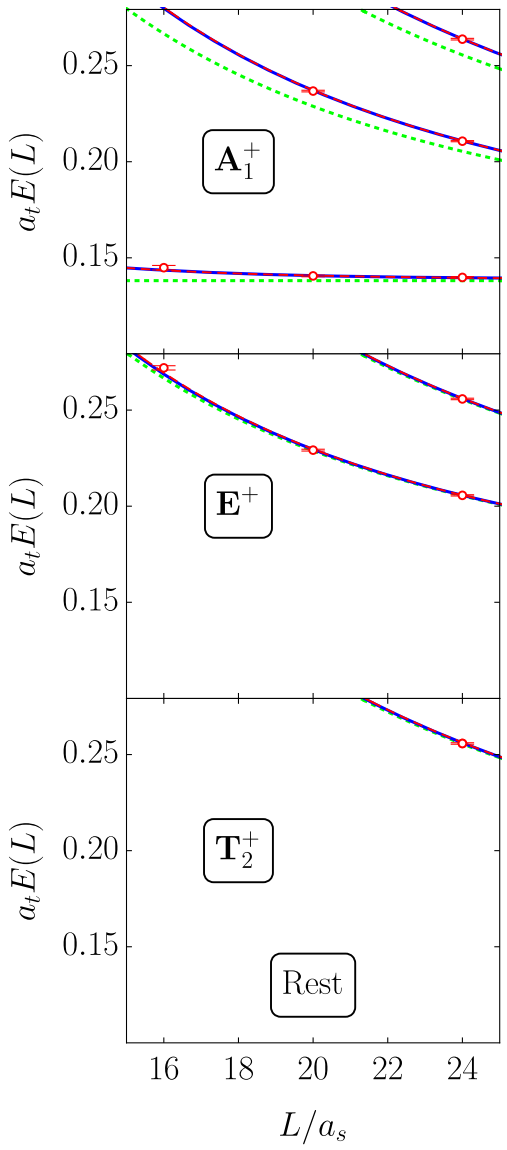

FIG. 2. Rest-frame finite-volume spectrum fit of the separable potential model to the lattice QCD results of Ref. [34] for isospin-2 $\pi\pi$ scattering. Red dashed (rest-only fit) and blue solid (rest and moving fit) curves illustrate the energies resolved in the separable potential model as the fit parameters of Table IV are optimized to fit the lattice QCD results (red points in this figure and blue points in Fig. 3). Results of the rest-only and rest and moving fits are almost indistinguishable. Green dotted curves illustrate the noninteracting pion-pair energies.

$$\chi^2 = [E_{\rm Sep} - E_{\rm Lattice}]^T [\mathbb{C}]^{-1} [E_{\rm Sep} - E_{\rm Lattice}], \quad (42)$$

where $E_{\rm Sep} - E_{\rm Lattice}$ denotes the vector of the differences between the spectrum obtained in the separable potential model and the lattice simulation. The covariance matrix $\mathbb{C}$ denotes the covariances in the lattice spectrum of Ref. [34].

The spectrum was calculated using the method discussed in Sec. III. While a momentum cutoff $N_{\rm cut} = 600$ was used in Ref. [12], we found that $N_{\rm cut} = 100$ is already enough for the analysis. Consider a specific level (we choose the highest one of A_1^+ in Fig. 2) for example, while the lattice level is 0.263773(424), the level solved from the Hamiltonian (using the parameters taken from the rest-frame fit in Ref. [12]) only shifts around 0.000001 when $N_{\rm cut}$ reduces from 600 to 100. Actually, for the lattice size $L \sim 3$ fm used here, $\frac{2\pi}{L}\sqrt{N_{\rm cut}}$ are roughly 10 and 4 GeV when $N_{\rm cut} = 600$ and 100 respectively. So $N_{\rm cut} = 100$ is totally enough here. For studies with larger L, however, one needs larger $N_{\rm cut}$. What is more, we found $|\chi^2_{N_{\rm cut}=100} - \chi^2_{N_{\rm cut}=600}| < 0.1$ in the range of parameters of interest. On the other hand, the values $a_t m_\pi = 0.06906(13)$ and $\xi = a_s/a_t = 3.444(6)$ may bring appreciable uncertainties to our analysis. Here we do not consider them, because the analysis based on the Lüscher method implemented in Ref. [34] suggests that they only have a small effect. The dimensions of the finite-volume Hamiltonian matrices for $N_{\rm cut} = 100$ and 600 are listed in Table III for each of the irreducible representations considered. Case B is not included, as we have $m_1 = m_2$ in the current $\pi\pi$ system. It is notable that the analysis of the moving-frame lattice data corresponds to the C2 case with $\eta = 1$.

B. The results

As in Ref. [12] we set $d_2 = d_4 = d_B = 4.78$ in the fitting. The results of the fit are shown in Table IV, where results of Ref. [12] are also included for comparison. Using those parameters, we predict the L-dependent spectrum for both rest and moving frames in Figs. 2 and 3.

TABLE III. The dimensions of the finite-volume Hamiltonian matrices for each of the irreducible representations Γ, for $N_{\rm cut} = 100$ and 600.

Case: **d**	Γ	$N_{\rm cut} = 100$	$N_{\rm cut} = 600$
A: (0,0,0)	$(A_1^+, A_2^+, E^+, T_1^+, T_2^+)$	(129, 0, 145, 75, 144)	(923, 0, 965, 488, 963)
C1: (0, 0, 1)	$(A_1^+, A_2^+, B_1^+, B_2^+, E^+)$	(357, 202, 271, 249, 448)	(4357, 3004, 3354, 3254, 6222)
C1: (0, 1, 1)	$(A_1^+, A_2^+, B_1^+, B_2^+)$	(624, 467, 465, 487)	(8122, 6806, 6802, 6923)
C1: (1, 1, 1)	(A_1^+, A_2^+, E^+)	(409, 239, 652)	(5320, 3504, 8879)
C2: (0, 0, 1)	$(A_1^+, A_2^+, B_1^+, B_2^+, E^+)$	(308, 173, 234, 214, 448)	(4102, 2826, 3158, 3064, 6222)
C2: (0, 1, 1)	$(A_1^+, A_2^+, B_1^+, B_2^+)$	(558, 420, 417, 433)	(7772, 6516, 6518, 6625)
C2: (1, 1, 1)	(A_1^+, A_2^+, E^+)	(354, 215, 564)	(5035, 3360, 8381)

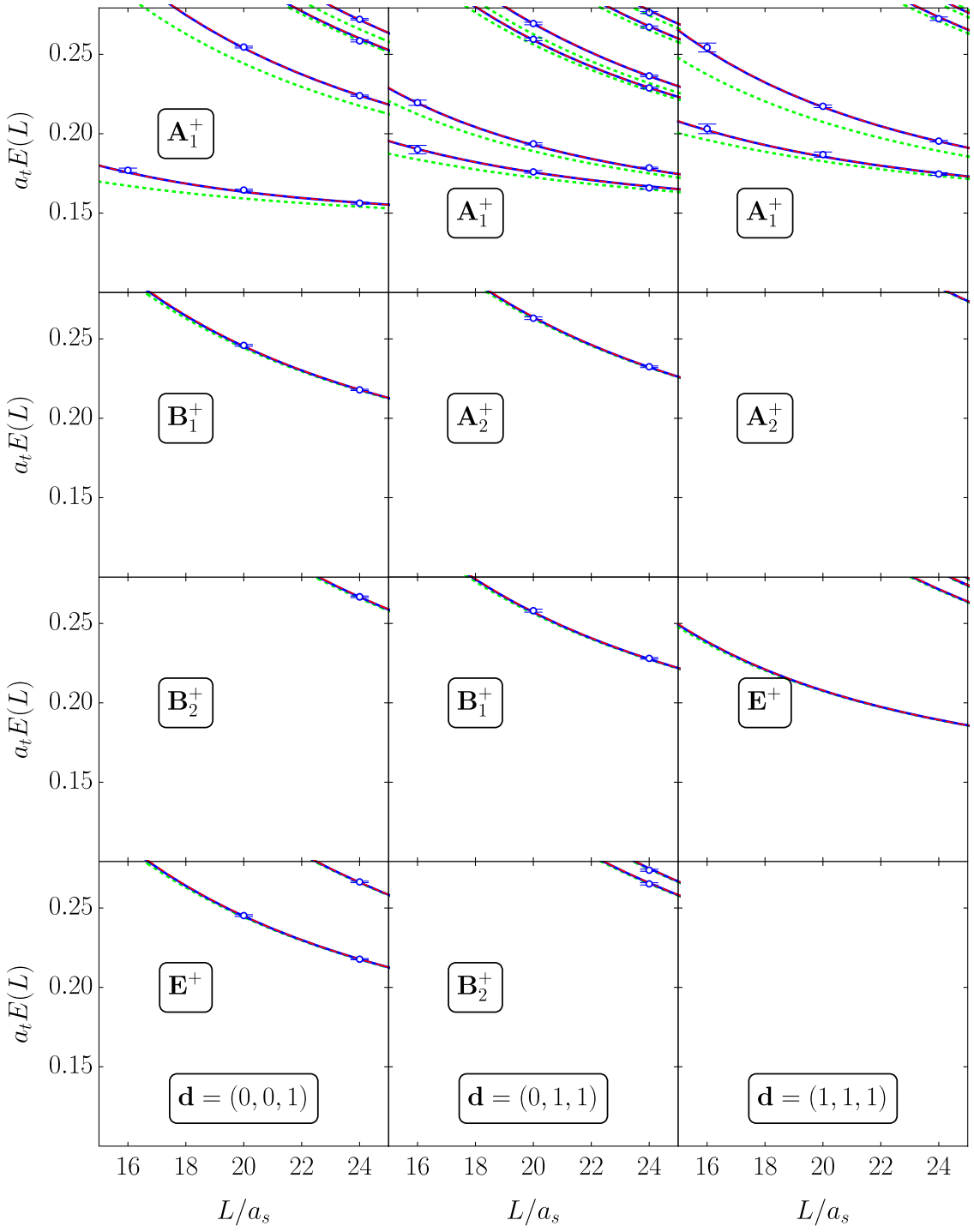

FIG. 3. As in Fig. 2 for moving-frame finite-volume spectrum.

TABLE IV. Parameters minimizing Eq. (42) with rest-frame data only and both rest- and moving-frame data. Both data are from Ref. [34] and the fitting results of rest-frame data are taken from Ref. [12]. Covariances for parameters are described by the Hessians listed in Eqs. (44) and (45).

		$\ell = 0$		$\ell = 2$		$\ell = 4$	
Data used	χ^2/N_{dof}	G_0	d_0	G_2	d_2	G_4	d_4
Rest only	$10.5/(11-4)$	67.8(3.4)	4.57(0.28)	90.6(28.3)	d_B	340.(307.)	d_B
Rest and moving	$115.9/(49-4)$	67.2(2.3)	4.59(0.18)	68.1(16.4)	d_B	257.(173.)	d_B

Our covariance for parameters λ_i is defined as $[\mathcal{H}/2]^{-1}$, where $\mathcal{H}$ is the Hessian of χ^2, the matrix of second-order partial derivatives over parameters

$$[\mathcal{H}]_{i,j} = \frac{\partial^2 \chi^2}{\partial \lambda_i \partial \lambda_j}. \tag{43}$$

As two d_l are fixed, we only have four parameters and the final covariance returned by MINUIT 2 (ordered as G_0, d_0, G_2, G_4) is

$$[\mathcal{H}/2]^{-1} = \begin{bmatrix} \underline{5.28} & \underline{0.321} & 21.1 & 47.3 \\ \underline{0.321} & \underline{0.0323} & 0.839 & 3.78 \\ 21.1 & 0.839 & \underline{269.} & 716. \\ 47.3 & 3.78 & 716. & \underline{2.99\times10^4} \end{bmatrix}. \tag{44}$$

For comparison, we also list the covariance obtained in Ref. [12] for the fitting of rest-frame data:

$$[\mathcal{H}_{\mathrm{Rest}}/2]^{-1} = \begin{bmatrix} \underline{11.4} & \underline{0.674} & 58.4 & -197. \\ \underline{0.674} & \underline{0.0773} & 1.53 & -9.61 \\ 58.4 & 1.53 & \underline{802.} & -1.28\times10^3 \\ -197. & -9.61 & -1.28\times10^3 & \underline{9.45\times10^4} \end{bmatrix}. \tag{45}$$

As the different values of l are decoupling in solving for the phase shifts, the values underlined in Eqs. (44) and (45) are used in calculating the errors in the phase shifts.

In Table IV, one may be concerned with the increase of χ^2/N_{dof} after including the moving frame data. However, the fitting based on the Lüscher method implemented in Ref. [34] gives $\chi^2/N_{\mathrm{dof}} = 116/(49-3)$ (they did not include the g-wave), quite close to ours. As shown in Fig. 4, the inclusion of moving frame lattice QCD results induces small variations in the phase shifts within the 1σ uncertainties of the predictions from the rest-frame data alone. However, the use of moving-frame data reduces the uncertainties in the HEFT phase shifts significantly. Moreover, the constraints provided by several lattice QCD energy levels on a small number of parameters characterizing the spectrum lead to results that are relatively precise in comparison to the Lüscher method. Still the results from the two approaches are generally consistent with only one outlier arising from the Lüscher method.

We also examine the differences in the finite-volume spectra associated with the elongation of the lattice volume versus the nonzero total momentum of the two-particle system. Our consideration aims to understand how elongation and nonzero total momentum differ in the spectrum. One may find for the pure elongated and the pure moving systems that $\frac{1}{\eta}$ and γ play a similar role.

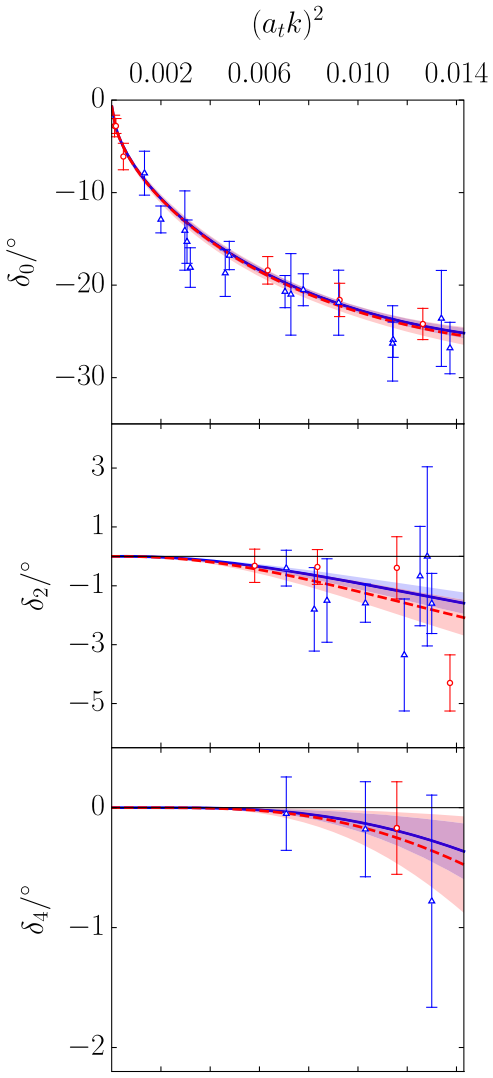

FIG. 4. Phase shift curves predicted by the HEFT separable potential model for s (top), d (middle) and g (bottom) partial waves are compared with points determined via Lüscher's method in Ref. [34]. Red dashed (blue solid) curves illustrate the central values of the phase shifts obtained from rest-frame data only (both rest- and moving-frame data). The colored shading describes the associated 1σ uncertainties. The red circle (blue triangle) points from Ref. [34] illustrate the phase shifts that can be extracted from the finite-volume spectrum of Figs. 2 and 3 using Lüscher's method.

Noting that γ depends on the momentum $\mathbf{k}$ and the total momentum $\mathbf{P}$, to make a comparison we set $\eta = \frac{1}{\gamma} \approx 0.868$ with γ taking the value on $\mathbf{k} = 0$, $\mathbf{d} = (0,0,1)$ and $L/a_s = 20$. We predict the L-dependent spectrum for the corresponding elongated, moving and elongated moving systems in Fig. 5. These three systems provide quite different spectra. Thus the consideration of elongated, moving, and elongated-moving systems are useful for generating more data within a certain range of lattice sizes.

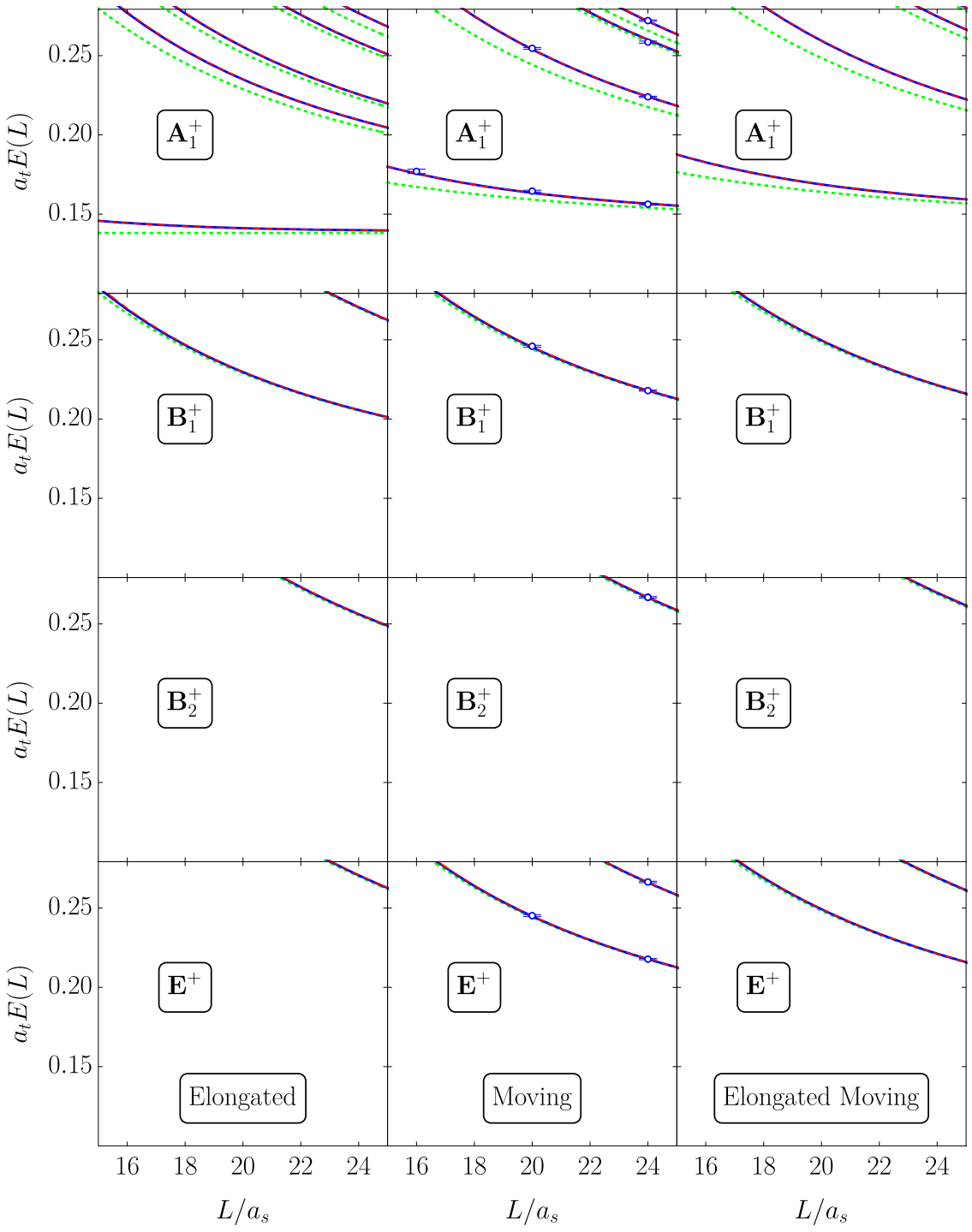

FIG. 5. As in Fig. 2 for elongated, moving and elongated moving systems with $\eta \approx 0.868$ and $\mathbf{d} = (0, 0, 1)$.

V. SUMMARY

In this work, we have extended HEFT to accommodate both an elongated finite volume and systems with nonzero total momentum. We also consider their combination when the directions of the elongation and the total momentum are aligned. To calculate the finite-volume energy levels, we first constructed the elongated-moving Hamiltonian Eqs. (17)–(20) via the potential parametrized in the rest frame. The spectrum solved from the Hamiltonian can approximate the real spectrum of the elongated moving system up to exponentially suppressed corrections. The elongation was handled in the usual way, and the moving effects were realized via a momentum transformation proposed in Ref. [31].

We then applied the formalism proposed in Ref. [12] to disentangle the partial-wave mixing in the elongated moving Hamiltonian. This formalism maximally reduces the dimension of the Hamiltonian matrix. Different from the rest frame, the elongated moving system has an additional characteristic direction, which prefers the partial-wave expansion expanded in a specific coordinate system.

Next, an example of isospin-2 $\pi\pi$ scattering was used to demonstrate how this formalism works. The use of moving-frame data induced small corrections in the phase shifts within the 1σ bounds of the rest-frame predictions. However the consideration of moving-frame lattice results significantly reduced the uncertainty in the phase-shift predictions. The consistency between analyses from the rest-frame Hamiltonian formalism implemented in Ref. [12] and the Lüscher method implemented in Ref. [34] is maintained by the moving-frame Hamiltonian formalism implemented here.

Finally, we examined differences between the effects of elongation and nonzero total momentum. The spectra obtained from the elongated, moving and elongated moving systems are quite different, and provide additional avenues for generating more lattice QCD results within a certain range of lattice size. On the current status of lattice simulations, L is roughly in the range 2–6 fm.

This work has largely accomplished the outlook of Ref. [12] for the generalization of the Hamiltonian formalism. More applications to two-body channels with data from elongated and moving systems are planned. Furthermore, as mentioned in Ref. [12], the moving-frame formalism developed here is necessary for a three-body formalism, since two of the three particles can have a nonvanishing total momentum. In the three-body case, a direct Hamiltonian fit should be formally simpler than the three-body Lüscher formalism. Of course, one of the remaining challenges is the significant increase in the dimension of the resultant Hamiltonian matrix.

ACKNOWLEDGMENTS

The finite-volume energy levels and their covariances from Ref. [34] were provided by the Hadron Spectrum collaboration—no endorsement on their part of the analysis presented in the current paper should be assumed. We thank Frank X. Lee, Ross D. Young and James M. Zanotti for comments and discussions. This work is also supported by the Fundamental Research Funds for the Central Universities. This research was supported by the Australian Research Council through ARC Discovery Project Grants No. DP150103101 and No. DP180100497 (A. W. T.) and No. DP150103164, No. DP190102215 and No. DP210103706 (D. B. L.).

APPENDIX A: SYMMETRY GROUPS RELEVANT TO FINITE VOLUME

In the infinite volume, with the symmetry group G_∞ and its irreducible representations (irreps) Γ_∞, one can label the quantum state vectors as $|\Gamma_\infty, \alpha_\infty\rangle$, where α_∞ is the index for the vectors in the irrep Γ_∞. For example, if we consider $G_\infty = SO(3)$, then $|\Gamma_\infty, \alpha_\infty\rangle$ will be $|l, m\rangle$. In the finite volume, the symmetry group G_∞ reduces into one of its subgroups G, and the vectors for an irrep Γ are now labeled as $|\Gamma, \alpha\rangle$.

According to the restricted representation, the infinite-volume vectors $|\Gamma_\infty, \alpha_\infty\rangle$ also behave as the vectors belonging to the representations of G, hence, they can be combined to obtain the vectors belonging to the irrep Γ as follows:

$$|\Gamma, f, \alpha\rangle = \sum_{\alpha_\infty} [C_{\Gamma_\infty}]_{\alpha_\infty;\Gamma,f,\alpha} |\Gamma_\infty, \alpha_\infty\rangle, \tag{A1}$$

where f is introduced since a specific Γ can be obtained more than once from the reduction of a single Γ_∞. C_{Γ_∞} is the unitary coefficient matrix. The purpose of this section is to provide some frequently used C_{Γ_∞}. The results are summarized in Tables VI to XIII.

Roughly speaking, bosons and fermions can be classified by the single-valued and double-valued irreps of the group O(3) respectively. The group O(3) is isomorphic to $\mathrm{SO}(3) \times \mathrm{C}_2$ where the C_2 is generated by the parity inversion. The relation can be formally written as

$$[\mathrm{O}(3)] = [\mathrm{SO}(3)] \times \left\{ \begin{bmatrix} 1 & & \\ & 1 & \\ & & 1 \end{bmatrix}, \begin{bmatrix} -1 & & \\ & -1 & \\ & & -1 \end{bmatrix} \right\}. \tag{A2}$$

In the elongated moving system, one also cares about the group $\mathrm{O}(2) \times \mathrm{C}_2$. It can be formally written as

$$\begin{bmatrix} \mathrm{O}(2) & \\ & 1 \end{bmatrix} \times \left\{ \begin{bmatrix} 1 & & \\ & 1 & \\ & & 1 \end{bmatrix}, \begin{bmatrix} -1 & & \\ & -1 & \\ & & -1 \end{bmatrix} \right\}. \tag{A3}$$

The group O(2) is isomorphic to the semidirect product $\mathrm{SO}(2) \rtimes \mathrm{C}_2$ formally written as

$$\begin{bmatrix} \mathrm{O}(2) & \\ & 1 \end{bmatrix} = \begin{bmatrix} \mathrm{SO}(2) & \\ & 1 \end{bmatrix} \rtimes \left\{ \begin{bmatrix} 1 & & \\ & 1 & \\ & & 1 \end{bmatrix}, \begin{bmatrix} 1 & & \\ & -1 & \\ & & 1 \end{bmatrix} \right\}, \tag{A4}$$

where the C_2 is generated by the reflection rather than the parity inversion.

Since the irreps of direct-product groups can be constructed as the tensor products of the irreps of the two original groups, we will focus on the groups without the parity inversion in the following discussions, that are, SO(3) and O(2). Although the irreps of SO(3) and O(2) are both labeled as integers and half-integers, they have

TABLE V. Groups and irreps.

G_∞	Γ_∞ (boson)	Γ_∞ (fermion)	**d**	G	Γ (boson)	Γ (fermion)
SO(3)	$0, 1, 2, \ldots$	$\frac{1}{2}, \frac{3}{2}, \frac{5}{2}, \ldots$	(0, 0, 0)	O	A_1, A_2, E, T_1, T_2	G_1, G_2, H
O(2)	$0, 1, 2, \ldots$	$\frac{1}{2}, \frac{3}{2}, \frac{5}{2}, \ldots$	(0, 0, 1)	Dih_4	A_1, A_2, B_1, B_2, E	G_1, G_2
			(0, 1, 1)	Dih_2	A_1, A_2, B_1, B_2	G
			(1, 1, 1)	Dih_3	A_1, A_2, E	K_1, K_2, G

different dimensions. For SO(3), α_∞ takes $-\Gamma_\infty$, $-\Gamma_\infty+1, \ldots, \Gamma_\infty$, so the dimension will be $2\Gamma_\infty+1$. For O(2), α_∞ can only take $+$ when $\Gamma_\infty=0$, and can take both $+$ and $-$ in other cases.

In the finite volume, SO(3) will reduce into the octahedral group O, and O(2) will reduce into dihedral groups whose orders will depend on the direction of the elongated moving vector **d**. Groups and their irreps are summarized in Table V, where A, B and K are labels for one-dimensional irreps, E and G for two dimensional, T for three dimensional, and H for four dimensional.

TABLE VI. C_{Γ_∞} for bosonic irreps of SO(3) taken from Table A.2 of Ref. [77].

Γ_∞	Γ	α	$\sum_{\alpha_\infty}[C_{\Gamma_\infty}]_{\alpha_\infty;\Gamma,f\equiv1,\alpha}\lvert\Gamma_\infty,\alpha_\infty\rangle$
0	A_1	1	$\lvert0,0\rangle$
1	T_1	1	$\frac{1}{\sqrt{2}}(\lvert1,-1\rangle-\lvert1,1\rangle)$
		2	$\frac{i}{\sqrt{2}}(\lvert1,-1\rangle+\lvert1,1\rangle)$
		3	$\lvert1,0\rangle$
2	E	1	$\lvert2,0\rangle$
		2	$\frac{1}{\sqrt{2}}(\lvert2,-2\rangle+\lvert2,2\rangle)$
	T_2	1	$-\frac{1}{\sqrt{2}}(\lvert2,-1\rangle+\lvert2,1\rangle)$
		2	$\frac{i}{\sqrt{2}}(\lvert2,-1\rangle-\lvert2,1\rangle)$
		3	$-\frac{1}{\sqrt{2}}(\lvert2,-2\rangle-\lvert2,2\rangle)$
3	A_2	1	$\frac{1}{\sqrt{2}}(\lvert3,-2\rangle-\lvert3,2\rangle)$
	T_1	1	$\frac{\sqrt{5}}{4}(\lvert3,-3\rangle-\lvert3,3\rangle)-\frac{\sqrt{3}}{4}(\lvert3,-1\rangle-\lvert3,1\rangle)$
		2	$\frac{-i\sqrt{5}}{4}(\lvert3,-3\rangle+\lvert3,3\rangle)-\frac{i\sqrt{3}}{4}(\lvert3,-1\rangle+\lvert3,1\rangle)$
		3	$\lvert3,0\rangle$
	T_2	1	$-\frac{\sqrt{3}}{4}(\lvert3,-3\rangle-\lvert3,3\rangle)-\frac{\sqrt{5}}{4}(\lvert3,-1\rangle-\lvert3,1\rangle)$
		2	$\frac{-i\sqrt{3}}{4}(\lvert3,-3\rangle+\lvert3,3\rangle)+\frac{i\sqrt{5}}{4}(\lvert3,-1\rangle+\lvert3,1\rangle)$
		3	$\frac{1}{\sqrt{2}}(\lvert3,-2\rangle+\lvert3,2\rangle)$
4	A_1	1	$\frac{\sqrt{30}}{12}(\lvert4,-4\rangle+\lvert4,4\rangle)+\frac{\sqrt{21}}{6}\lvert4,0\rangle$
	E	1	$-\frac{\sqrt{42}}{12}(\lvert4,-4\rangle+\lvert4,4\rangle)+\frac{\sqrt{15}}{6}\lvert4,0\rangle$
		2	$-\frac{1}{\sqrt{2}}(\lvert4,-2\rangle+\lvert4,2\rangle)$
	T_1	1	$-\frac{1}{4}(\lvert4,-3\rangle+\lvert4,3\rangle)-\frac{\sqrt{7}}{4}(\lvert4,-1\rangle+\lvert4,1\rangle)$
		2	$\frac{i}{4}(\lvert4,-3\rangle-\lvert4,3\rangle)-\frac{i\sqrt{7}}{4}(\lvert4,-1\rangle-\lvert4,1\rangle)$
		3	$\frac{1}{\sqrt{2}}(\lvert4,-4\rangle-\lvert4,4\rangle)$
	T_2	1	$\frac{\sqrt{7}}{4}(\lvert4,-3\rangle+\lvert4,3\rangle)-\frac{1}{4}(\lvert4,-1\rangle+\lvert4,1\rangle)$
		2	$\frac{i\sqrt{7}}{4}(\lvert4,-3\rangle-\lvert4,3\rangle)+\frac{i}{4}(\lvert4,-1\rangle-\lvert4,1\rangle)$
		3	$\frac{1}{\sqrt{2}}(\lvert4,-2\rangle-\lvert4,2\rangle)$

For SO(3), those C_{Γ_∞} are provided in many papers, e.g., Table A.2 (for bosons) and Table A.4 (for fermions) of Ref. [77]. Here we cite their results in Tables VI and VII.

For O(2), we take the case $\mathbf{d}=(0,0,1)$ for example. The rotations of angles $0, \frac{\pi}{2}, \pi$ and $\frac{3\pi}{2}$ in the SO(2) and the reflection in C_2 will survive, then the resulting group Dih_4 can be formally written as $C_4 \rtimes C_2$. So Dih_4 can be generated by the $\frac{\pi}{2}$ rotation element $R_{\frac{\pi}{2}}$ and the reflection element R, whose representation matrices can be chosen to be

$$R_{\frac{\pi}{2}}^{\Gamma_\infty=0}=[1], \qquad R_{\frac{\pi}{2}}^{\Gamma_\infty\neq0}=\begin{bmatrix} e^{i\Gamma_\infty\frac{\pi}{2}} & 0 \\ 0 & e^{-i\Gamma_\infty\frac{\pi}{2}} \end{bmatrix},$$
$$R^{\Gamma_\infty=0}=[1], \qquad R^{\Gamma_\infty\neq0}=\begin{bmatrix} 0 & 1 \\ 1 & 0 \end{bmatrix}, \tag{A5}$$

TABLE VII. C_{Γ_∞} for fermionic irreps of SO(3) taken from Table A.4 of Ref. [77].

Γ_∞	Γ	α	$\sum_{\alpha_\infty}[C_{\Gamma_\infty}]_{\alpha_\infty;\Gamma,f\equiv1,\alpha}\lvert\Gamma_\infty,\alpha_\infty\rangle$
$\frac{1}{2}$	G_1	1	$\lvert\frac{1}{2},\frac{1}{2}\rangle$
		2	$\lvert\frac{1}{2},-\frac{1}{2}\rangle$
$\frac{3}{2}$	H	1	$\lvert\frac{3}{2},\frac{3}{2}\rangle$
		2	$\lvert\frac{3}{2},\frac{1}{2}\rangle$
		3	$\lvert\frac{3}{2},-\frac{1}{2}\rangle$
		4	$\lvert\frac{3}{2},-\frac{3}{2}\rangle$
$\frac{5}{2}$	G_2	1	$\frac{\sqrt{30}}{6}\lvert\frac{5}{2},-\frac{3}{2}\rangle-\frac{\sqrt{6}}{6}\lvert\frac{5}{2},\frac{5}{2}\rangle$
		2	$-\frac{\sqrt{6}}{6}\lvert\frac{5}{2},-\frac{5}{2}\rangle+\frac{\sqrt{30}}{6}\lvert\frac{5}{2},\frac{3}{2}\rangle$
	H	1	$-\frac{\sqrt{30}}{6}\lvert\frac{5}{2},-\frac{5}{2}\rangle-\frac{\sqrt{6}}{6}\lvert\frac{5}{2},\frac{3}{2}\rangle$
		2	$\lvert\frac{5}{2},\frac{1}{2}\rangle$
		3	$-\lvert\frac{5}{2},-\frac{1}{2}\rangle$
		4	$\frac{\sqrt{6}}{6}\lvert\frac{5}{2},-\frac{3}{2}\rangle+\frac{\sqrt{30}}{6}\lvert\frac{5}{2},\frac{5}{2}\rangle$
$\frac{7}{2}$	G_1	1	$\frac{\sqrt{15}}{6}\lvert\frac{7}{2},-\frac{7}{2}\rangle+\frac{\sqrt{21}}{6}\lvert\frac{7}{2},\frac{1}{2}\rangle$
		2	$-\frac{\sqrt{21}}{6}\lvert\frac{7}{2},-\frac{1}{2}\rangle-\frac{\sqrt{15}}{6}\lvert\frac{7}{2},\frac{7}{2}\rangle$
	G_2	1	$-\frac{1}{2}\lvert\frac{7}{2},-\frac{3}{2}\rangle+\frac{\sqrt{3}}{2}\lvert\frac{7}{2},\frac{5}{2}\rangle$
		2	$-\frac{\sqrt{3}}{2}\lvert\frac{7}{2},-\frac{5}{2}\rangle+\frac{1}{2}\lvert\frac{7}{2},\frac{3}{2}\rangle$
	H	1	$\frac{1}{2}\lvert\frac{7}{2},-\frac{5}{2}\rangle+\frac{\sqrt{3}}{2}\lvert\frac{7}{2},\frac{3}{2}\rangle$
		2	$\frac{\sqrt{21}}{6}\lvert\frac{7}{2},-\frac{7}{2}\rangle-\frac{\sqrt{15}}{6}\lvert\frac{7}{2},\frac{1}{2}\rangle$
		3	$-\frac{\sqrt{15}}{6}\lvert\frac{7}{2},-\frac{1}{2}\rangle+\frac{\sqrt{21}}{6}\lvert\frac{7}{2},\frac{7}{2}\rangle$
		4	$\frac{\sqrt{3}}{2}\lvert\frac{7}{2},-\frac{3}{2}\rangle+\frac{1}{2}\lvert\frac{7}{2},\frac{5}{2}\rangle$

where we represent $|\Gamma_\infty \neq 0, \pm\rangle$ as follows:

$$|\Gamma_\infty \neq 0, -\rangle \sim \begin{bmatrix} 1 \\ 0 \end{bmatrix}, \qquad |\Gamma_\infty \neq 0, +\rangle \sim \begin{bmatrix} 0 \\ 1 \end{bmatrix}. \tag{A6}$$

Note when $\Gamma_\infty \neq 0$, since Γ_∞ and $\Gamma_\infty + 4$ share the same representation matrices as indicated in Eq. (A5), one will have $C_{\Gamma_\infty} = C_{\Gamma_\infty+4}$. In fact, for $\mathbf{d} = (0, 1, 1)$, it will be $C_{\Gamma_\infty} = C_{\Gamma_\infty+2}$, and for $\mathbf{d} = (1, 1, 1)$, it will be $C_{\Gamma_\infty} = C_{\Gamma_\infty+3}$. Because those irreps are only one or two dimensional, it is easy to find out those C_{Γ_∞}. We also note that since there is still the freedom to choose the representation matrices of the finite-volume irreps, those C_{Γ_∞} are not unique. The results for our choice are summarized in Tables VIII to XIII.

1. States in elongated moving system

In the elongated moving system, one will deal with the states

TABLE VIII. C_{Γ_∞} for bosonic irreps of O(2) when $\mathbf{d} = (0, 0, 1)$, and $C_{\Gamma_\infty} = C_{\Gamma_\infty+4}$ for $\Gamma_\infty \neq 0$.

Γ_∞	Γ	α	$\sum_{\alpha_\infty}[C_{\Gamma_\infty}]_{\alpha_\infty;\Gamma,f\equiv1,\alpha}\lvert\Gamma_\infty,\alpha_\infty\rangle$
0	A_1	1	$\lvert 0,+\rangle$
1	E	1	$\lvert 1,-\rangle$
		2	$\lvert 1,+\rangle$
2	B_1	1	$\frac{1}{\sqrt{2}}(\lvert 2,-\rangle + \lvert 2,+\rangle)$
	B_2	1	$\frac{1}{\sqrt{2}}(\lvert 2,-\rangle - \lvert 2,+\rangle)$
3	E	1	$\lvert 3,+\rangle$
		2	$\lvert 3,-\rangle$
4	A_1	1	$\frac{1}{\sqrt{2}}(\lvert 4,-\rangle + \lvert 4,+\rangle)$
	A_2	1	$\frac{1}{\sqrt{2}}(\lvert 4,-\rangle - \lvert 4,+\rangle)$

TABLE IX. C_{Γ_∞} for fermionic irreps of O(2) when $\mathbf{d} = (0, 0, 1)$, and $C_{\Gamma_\infty} = C_{\Gamma_\infty+4}$ for $\Gamma_\infty \neq 0$.

Γ_∞	Γ	α	$\sum_{\alpha_\infty}[C_{\Gamma_\infty}]_{\alpha_\infty;\Gamma,f\equiv1,\alpha}\lvert\Gamma_\infty,\alpha_\infty\rangle$
$\frac{1}{2}$	G_1	1	$\lvert\frac{1}{2},-\rangle$
		2	$\lvert\frac{1}{2},+\rangle$
$\frac{3}{2}$	G_2	1	$\lvert\frac{3}{2},-\rangle$
		2	$\lvert\frac{3}{2},+\rangle$
$\frac{5}{2}$	G_2	1	$\lvert\frac{5}{2},+\rangle$
		2	$\lvert\frac{5}{2},-\rangle$
$\frac{7}{2}$	G_1	1	$\lvert\frac{7}{2},+\rangle$
		2	$\lvert\frac{7}{2},-\rangle$

TABLE X. C_{Γ_∞} for bosonic irreps of O(2) when $\mathbf{d} = (0, 1, 1)$, and $C_{\Gamma_\infty} = C_{\Gamma_\infty+2}$ for $\Gamma_\infty \neq 0$.

Γ_∞	Γ	α	$\sum_{\alpha_\infty}[C_{\Gamma_\infty}]_{\alpha_\infty;\Gamma,f\equiv1,\alpha}\lvert\Gamma_\infty,\alpha_\infty\rangle$
0	A_1	1	$\lvert 0,+\rangle$
1	B_1	1	$\frac{1}{\sqrt{2}}(\lvert 1,-\rangle + \lvert 1,+\rangle)$
	B_2	1	$\frac{1}{\sqrt{2}}(\lvert 1,-\rangle - \lvert 1,+\rangle)$
2	A_1	1	$\frac{1}{\sqrt{2}}(\lvert 2,-\rangle + \lvert 2,+\rangle)$
	A_2	1	$\frac{1}{\sqrt{2}}(\lvert 2,-\rangle - \lvert 2,+\rangle)$

TABLE XI. C_{Γ_∞} for fermionic irreps of O(2) when $\mathbf{d} = (0, 1, 1)$, and $C_{\Gamma_\infty} = C_{\Gamma_\infty+2}$ for $\Gamma_\infty \neq 0$.

Γ_∞	Γ	α	$\sum_{\alpha_\infty}[C_{\Gamma_\infty}]_{\alpha_\infty;\Gamma,f\equiv1,\alpha}\lvert\Gamma_\infty,\alpha_\infty\rangle$
$\frac{1}{2}$	G	1	$\lvert\frac{1}{2},-\rangle$
		2	$\lvert\frac{1}{2},+\rangle$
$\frac{3}{2}$	G	1	$\lvert\frac{3}{2},+\rangle$
		2	$\lvert\frac{3}{2},-\rangle$

TABLE XII. C_{Γ_∞} for bosonic irreps of O(2) when $\mathbf{d} = (1, 1, 1)$, and $C_{\Gamma_\infty} = C_{\Gamma_\infty+3}$ for $\Gamma_\infty \neq 0$.

Γ_∞	Γ	α	$\sum_{\alpha_\infty}[C_{\Gamma_\infty}]_{\alpha_\infty;\Gamma,f\equiv1,\alpha}\lvert\Gamma_\infty,\alpha_\infty\rangle$
0	A_1	1	$\lvert 0,+\rangle$
1	E	1	$\lvert 1,-\rangle$
		2	$\lvert 1,+\rangle$
2	E	1	$\lvert 2,+\rangle$
		2	$\lvert 2,-\rangle$
3	A_1	1	$\frac{1}{\sqrt{2}}(\lvert 3,-\rangle + \lvert 3,+\rangle)$
	A_2	1	$\frac{1}{\sqrt{2}}(\lvert 3,-\rangle - \lvert 3,+\rangle)$

TABLE XIII. C_{Γ_∞} for fermionic irreps of O(2) when $\mathbf{d} = (1, 1, 1)$, and $C_{\Gamma_\infty} = C_{\Gamma_\infty+3}$ for $\Gamma_\infty \neq 0$.

Γ_∞	Γ	α	$\sum_{\alpha_\infty}[C_{\Gamma_\infty}]_{\alpha_\infty;\Gamma,f\equiv1,\alpha}\lvert\Gamma_\infty,\alpha_\infty\rangle$
$\frac{1}{2}$	G	1	$\lvert\frac{1}{2},-\rangle$
		2	$\lvert\frac{1}{2},+\rangle$
$\frac{3}{2}$	K_1	1	$\frac{1}{\sqrt{2}}(\lvert\frac{3}{2},-\rangle + \lvert\frac{3}{2},+\rangle)$
	K_2	1	$\frac{1}{\sqrt{2}}(\lvert\frac{3}{2},-\rangle - \lvert\frac{3}{2},+\rangle)$
$\frac{5}{2}$	G	1	$\lvert\frac{5}{2},+\rangle$
		2	$\lvert\frac{5}{2},-\rangle$

TABLE XIV. $(\tilde{\mathbf{x}}, \tilde{\mathbf{y}}, \tilde{\mathbf{z}})$ for different $\mathbf{d}$.

$\mathbf{d}$	$\tilde{\mathbf{x}}$	$\tilde{\mathbf{y}}$	$\tilde{\mathbf{z}}$
(0, 0, 1)	(1, 0, 0)	(0, 1, 0)	(0, 0, 1)
(0, 1, 1)	(1, 0, 0)	$\frac{1}{\sqrt{2}}(0,1,-1)$	$\frac{1}{\sqrt{2}}(0,1,1)$
(1, 1, 1)	$\frac{1}{\sqrt{6}}(2,-1,-1)$	$\frac{1}{\sqrt{2}}(0,1,-1)$	$\frac{1}{\sqrt{3}}(1,1,1)$

$$|e_n;\Gamma_\infty,\alpha_\infty\rangle := \sum_{\hat{e}_n} e^{im\phi}|\mathbf{n}\rangle, \tag{A7}$$

where e_n denotes $(\mathbf{n}^2, \mathbf{n}\cdot\mathbf{d})$, and $\sum_{\hat{e}_n}$ means summing over all the states with the same e_n, and $(\Gamma_\infty, \alpha_\infty)$ will be $(|m|, \mathrm{sign}(m))$ [we define $\mathrm{sign}(0) = +$], and the angle ϕ depends on the choice of the axes labeled as $(\tilde{\mathbf{x}}, \tilde{\mathbf{y}}, \tilde{\mathbf{z}})$, which can differ from the finite-volume box's axes $(\mathbf{x}, \mathbf{y}, \mathbf{z})$. The purpose of this section is to find out some suitable choices for $(\tilde{\mathbf{x}}, \tilde{\mathbf{y}}, \tilde{\mathbf{z}})$ so that the representation matrices of the symmetry group are consistent with Eq. (A5) (and its counterparts for other $\mathbf{d}$) and hence the C_{Γ_∞} provided before can be used. The results are summarized in Table XIV.

We take the case $\mathbf{d} = (0, 0, 1)$ for example as before. One can first choose $\tilde{\mathbf{z}}$ to be the normalized elongated moving vector $\mathbf{d}/|\mathbf{d}|$, and also chooses the rotation axis of R_{ϕ_0} in the SO(2) to be $\tilde{\mathbf{z}}$, then only rotations of angles $0, \frac{\pi}{2}, \pi$ and $\frac{3\pi}{2}$ will always send an integer vector to another integer vector as expected. So one has

$$R_{\phi_0}|e_n;\Gamma_\infty,\alpha_\infty\rangle = e^{-im\phi_0}|e_n;\Gamma_\infty,\alpha_\infty\rangle \tag{A8}$$

for ϕ_0 to be $0, \frac{\pi}{2}, \pi$ or $\frac{3\pi}{2}$, which is consistent with Eq. (A5). One then chooses the reversion axis of R in the C_2 to be $\tilde{\mathbf{x}}$, so R will send $\mathbf{n}$ to $\mathbf{n} - 2(\mathbf{n}\cdot\tilde{\mathbf{y}})\tilde{\mathbf{y}}$. If $\tilde{\mathbf{y}}$ is chosen to make $2(\mathbf{n}\cdot\tilde{\mathbf{y}})\tilde{\mathbf{y}}$ an integer vector for any integer vector $\mathbf{n}$, one will have (for $\Gamma_\infty \neq 0$)

$$R|e_n;\Gamma_\infty,\alpha_\infty\rangle = |e_n;\Gamma_\infty,-\alpha_\infty\rangle, \tag{A9}$$

which is consistent with Eq. (A5). Our choices for $(\tilde{\mathbf{x}}, \tilde{\mathbf{y}}, \tilde{\mathbf{z}})$ are summarized in Table XIV.

APPENDIX B: SOLVING FOR THE P MATRIX

1. Rest-frame P matrix

With the usual definition of the spherical harmonics,

$$Y_{lm}(\hat{\mathbf{n}}) = \sqrt{\frac{2l+1}{4\pi}\frac{(l-m)!}{(l+m)!}}P_{lm}(\cos\theta)e^{im\phi},$$
$$P_{lm}(x) = \frac{(-1)^m}{2^l l!}(1-x^2)^{m/2}\frac{d^{l+m}}{dx^{l+m}}(x^2-1)^l \tag{B1}$$

and the definition of P matrix given in Ref. [12], the rest-frame P matrix will be

$$[P_{\mathbf{n}^2}]_{l',m';l,m} = 4\pi\sum_{\hat{\mathbf{n}}} Y^*_{l'm'}(\hat{\mathbf{n}})Y_{lm}(\hat{\mathbf{n}})$$
$$= c_{l',m';l,m}\sum_{n_z} P_{l'm'}(\cos\theta)P_{lm}(\cos\theta)$$
$$\times \sum_{n_x,n_y} e^{-i(m'-m)\phi}, \tag{B2}$$

where

$$c_{l',m';l,m} = \sqrt{(2l'+1)\frac{(l'-m')!}{(l'+m')!}}\sqrt{(2l+1)\frac{(l-m)!}{(l+m)!}}. \tag{B3}$$

When $\mathbf{n} = (0, 0, 0)$, the direction angles are ill defined, and we can set $Y_{lm} = \frac{\delta_{l0}}{\sqrt{4\pi}}$.

There are many useful properties of the P matrix listed as follows:

(i) $[P_{\mathbf{n}^2}]_{l',m';l,m}$ is real because of the symmetry under $\phi \to -\phi$.
(ii) $[P_{\mathbf{n}^2}]_{l',m';l,m} = 0$ when $l' + l$ is odd because of the symmetry under $\mathbf{n} \to -\mathbf{n}$.
(iii) $[P_{\mathbf{n}^2}]_{l',m';l,m} = 0$ when $m' + m$ is odd because of the symmetry under $\phi \to \phi + \pi$.
(iv) $[P_{\mathbf{n}^2}]_{l',m';l,m} = 0$ when $|m' - m| = 2$ because of the symmetry under $\phi \to \phi + \frac{\pi}{2}$.

The result of the summation

$$\sum_{n_x,n_y} e^{-i(m'-m)\phi} \tag{B4}$$

depends on $(\mathbf{n}^2, n_z)$. One need not calculate it for all $(\mathbf{n}^2, n_z)$ by noting the map $\mathbf{n} \to \pm\mathbf{n} + (0, 0, j)$ with any integer j. In fact, the summation Eq. (B4) is related to the P matrix $P^B_{e_n}$ with $\mathbf{d} = (0, 0, 1)$ discussed in Appendix B 2.

2. P matrix of the elongated moving system

From Eq. (33), the P matrix for the case B in Table II is

$$[P^B_{e_n}]_{|m'|,S'_m;|m|,S_m} = \sum_{\hat{e}_n} e^{-i(m'-m)\phi^*}, \tag{B5}$$

where it does not matter how to redefine the ill-defined ϕ^* when $\mathbf{n}^2 = \mathbf{n}_\parallel{}^2$, because either $m = m' = 0$ then Eq. (B5) is ϕ^*-independent, or one of m and m' is nonzero then $P_{l'm'}$ or P_{lm} in Table II and Eq. (B2) vanishes.

To solve for it, it is worth noting that the map $\mathbf{n} \to \mathbf{n} + j\mathbf{d}$ with $j\mathbf{d}$ any integer vector will tell us

$$P^B_{(\mathbf{n}^2,\mathbf{n}\cdot\mathbf{d})} = P^B_{(\mathbf{n}^2+2j\mathbf{n}\cdot\mathbf{d}+j^2\mathbf{d}^2,+\mathbf{n}\cdot\mathbf{d}+j\mathbf{d}^2)}, \tag{B6}$$

and the map $\mathbf{n} \to -\mathbf{n} + j\mathbf{d}$ will tell us

$$P^B_{(\mathbf{n}^2,\mathbf{n}\cdot\mathbf{d})} = (-1)^{m'-m} P^B_{(\mathbf{n}^2-2j\mathbf{n}\cdot\mathbf{d}+j^2\mathbf{d}^2,-\mathbf{n}\cdot\mathbf{d}+j\mathbf{d}^2)}. \tag{B7}$$

With the coordinate axes $(\tilde{x},\tilde{y},\tilde{z})$ of spherical harmonics taking the values in Table XIV, there are many useful properties of $P^B_{(\mathbf{n}^2,\mathbf{n}\cdot\mathbf{d})}$ listed as follows:

(i) $P^B_{(\mathbf{n}^2,\mathbf{n}\cdot\mathbf{d})}$ is real because of the symmetry under $\phi \to -\phi$, which holds for all the $\mathbf{d}$ presented in Table XIV.

(ii) $[P^B_{(\mathbf{n}^2,\mathbf{n}\cdot\mathbf{d})}]_{|m'|,S'_m;|m|,S_m} = 0$ when $m'+m$ is odd because of the symmetry under $\phi \to \phi+\pi$, which holds for $\mathbf{d} = (0,0,1),(0,1,1)$.

(iii) $[P^B_{(\mathbf{n}^2,\mathbf{n}\cdot\mathbf{d})}]_{|m'|,S'_m;|m|,S_m} = 0$ when $|m'-m| = 2$ because of the symmetry under $\phi \to \phi+\frac{\pi}{2}$, which holds only for $\mathbf{d} = (0,0,1)$.

For the case C (C1 or C2), the map $\mathbf{n} \to \mathbf{d}_\gamma - \mathbf{n}$ will tell us

$$[P^C_{e_n}]_{|m'|^\pm,S'_m;|m|^\mp,S_m} = 0, \tag{B8}$$

and

$$[P^C_{(\mathbf{n}^2,\{\mathbf{n}\cdot\mathbf{d},(\mathbf{d}_\gamma-\mathbf{n})\cdot\mathbf{d}\})}]_{|m'|^\pm,S'_m;|m|^\pm,S_m} = \begin{cases} 2[P^B_{(\mathbf{n}^2,\mathbf{n}\cdot\mathbf{d})}]_{|m'|,S'_m;|m|,S_m} & \mathbf{n}\cdot\mathbf{d} > \frac{\mathbf{d}_\gamma^2}{2} \\ [P^B_{(\mathbf{n}^2,\mathbf{n}\cdot\mathbf{d})}]_{|m'|,S'_m;|m|,S_m} & \mathbf{n}\cdot\mathbf{d} = \frac{\mathbf{d}_\gamma^2}{2} \\ 2(-1)^{m'-m}[P^B_{(\mathbf{n}^2,\mathbf{n}\cdot\mathbf{d})}]_{|m'|,S'_m;|m|,S_m} & \mathbf{n}\cdot\mathbf{d} < \frac{\mathbf{d}_\gamma^2}{2}, \end{cases} \tag{B9}$$

where we have used that $\cos\theta^*$ has the same sign with $\mathbf{n}\cdot\mathbf{d} - \frac{\mathbf{d}_\gamma^2}{2}$ in case C. We also emphasize that $P^{C1} \neq P^{C2}$ since $\mathbf{d}_\gamma = 0$ in case C1 while $\mathbf{d}_\gamma = \mathbf{d}$ in case C2.

[1] M. Lüscher, Commun. Math. Phys. **104**, 177 (1986).
[2] M. Lüscher, Commun. Math. Phys. **105**, 153 (1986).
[3] M. Lüscher, Nucl. Phys. **B354**, 531 (1991).
[4] J. M. M. Hall, A. C.-P. Hsu, D. B. Leinweber, A. W. Thomas, and R. D. Young, Phys. Rev. D **87**, 094510 (2013).
[5] J. M. M. Hall, W. Kamleh, D. B. Leinweber, B. J. Menadue, B. J. Owen, A. W. Thomas, and R. D. Young, Phys. Rev. Lett. **114**, 132002 (2015).
[6] J.-J. Wu, T.-S. H. Lee, A. W. Thomas, and R. D. Young, Phys. Rev. C **90**, 055206 (2014).
[7] Z.-W. Liu, W. Kamleh, D. B. Leinweber, F. M. Stokes, A. W. Thomas, and J.-J. Wu, Phys. Rev. Lett. **116**, 082004 (2016).
[8] Z.-W. Liu, W. Kamleh, D. B. Leinweber, F. M. Stokes, A. W. Thomas, and J.-J. Wu, Phys. Rev. D **95**, 034034 (2017).
[9] Z.-W. Liu, J. M. M. Hall, D. B. Leinweber, A. W. Thomas, and J.-J. Wu, Phys. Rev. D **95**, 014506 (2017).
[10] J.-J. Wu, H. Kamano, T.-S. H. Lee, D. B. Leinweber, and A. W. Thomas, Phys. Rev. D **95**, 114507 (2017).
[11] J.-J. Wu, D. B. Leinweber, Z.-W. Liu, and A. W. Thomas, Phys. Rev. D **97**, 094509 (2018).
[12] Y. Li, J.-J. Wu, C. D. Abell, D. B. Leinweber, and A. W. Thomas, Phys. Rev. D **101**, 114501 (2020).
[13] X. Feng, X. Li, and C. Liu, Phys. Rev. D **70**, 014505 (2004).
[14] X. Li and C. Liu, Phys. Lett. B **587**, 100 (2004).
[15] X. Li, Y. Chen, G.-Z. Meng, X. Feng, M. Gong, S. He, G. Li, C. Liu, Y.-B. Liu, J.-P. Ma, X.-F. Meng, Y. Shen, and J.-B. Zhang (CLQCD Collaboration), J. High Energy Phys. 07 (2007) 053.
[16] F. X. Lee and A. Alexandru, Phys. Rev. D **96**, 054508 (2017).
[17] N. Li, Y.-J. Wu, and Z.-W. Liu, Phys. Rev. D **97**, 014509 (2018).
[18] G.-Z. Meng, M. Gong, Y. Chen, S. He, G. Li, C. Liu, Y.-B. Liu, J.-P. Ma, X.-F. Meng, Z.-Y. Niu, Y. Shen, J.-B. Zhang, and Y.-J. Zhang (CLQCD Collaboration), Phys. Rev. D **80**, 034503 (2009).
[19] C. Pelissier and A. Alexandru, Phys. Rev. D **87**, 014503 (2013).
[20] D. Guo, A. Alexandru, R. Molina, and M. Döring, Phys. Rev. D **94**, 034501 (2016).
[21] D. Guo, A. Alexandru, R. Molina, M. Mai, and M. Döring, Phys. Rev. D **98**, 014507 (2018).
[22] C. Culver, M. Mai, A. Alexandru, M. Döring, and F. X. Lee, Phys. Rev. D **100**, 034509 (2019).
[23] C. Culver, M. Mai, R. Brett, A. Alexandru, and M. Döring, Phys. Rev. D **101**, 114507 (2020).
[24] Parallelepiped, https://en.wikipedia.org/wiki/File:Special_cases_of_parallelepiped.svg (2019).
[25] K. Rummukainen and S. Gottlieb, Nucl. Phys. **B450**, 397 (1995).
[26] C. Kim, C. Sachrajda, and S. R. Sharpe, Nucl. Phys. **B727**, 218 (2005).
[27] M. Göckeler, R. Horsley, M. Lage, U.-G. Meißner, P. E. L. Rakow, A. Rusetsky, G. Schierholz, and J. M. Zanotti, Phys. Rev. D **86**, 094513 (2012).
[28] Z. Davoudi and M. J. Savage, Phys. Rev. D **84**, 114502 (2011).
[29] Z. Fu, Phys. Rev. D **85**, 014506 (2012).
[30] L. Leskovec and S. Prelovsek, Phys. Rev. D **85**, 114507 (2012).
[31] Y. Li, J.-J. Wu, R. D. Young, and T.-S. H. Lee (to be published).
[32] J.-J. Wu, T.-S. H. Lee, D. B. Leinweber, A. W. Thomas, and R. D. Young, J. Phys. Soc. Jpn. Conf. Proc. **10**, 062002 (2016).
[33] T. D. Blanton and S. R. Sharpe, Phys. Rev. D **102**, 054520 (2020).

[34] J. J. Dudek, R. G. Edwards, and C. E. Thomas, Phys. Rev. D **86**, 034031 (2012).
[35] K. S. McElvain, Harmonic oscillator based effective theory, connecting LQCD to nuclear structure, Ph.D. thesis, UC Berkeley, 2017.
[36] K. McElvain and W. Haxton, Phys. Lett. B **797**, 134880 (2019).
[37] C. Drischler, W. Haxton, K. McElvain, E. Mereghetti, A. Nicholson, P. Vranas, and A. Walker-Loud, arXiv:1910.07961.
[38] V. Bernard, M. Lage, U.-G. Meißner, and A. Rusetsky, J. High Energy Phys. 11 (**2011**) 019.
[39] P. Guo, J. J. Dudek, R. G. Edwards, and A. P. Szczepaniak, Phys. Rev. D **88**, 014501 (2013).
[40] S. He, X. Feng, and C. Liu, J. High Energy Phys. 07 (2005) 011.
[41] B. Hu, R. Molina, M. Döring, and A. Alexandru, Phys. Rev. Lett. **117**, 122001 (2016).
[42] M. Lage, U.-G. Meissner, and A. Rusetsky, Phys. Lett. B **681**, 439 (2009).
[43] N. Li and C. Liu, Phys. Rev. D **87**, 014502 (2013).
[44] S. R. Beane, P. F. Bedaque, A. Parreno, and M. J. Savage, Phys. Lett. B **585**, 106 (2004).
[45] S. R. Beane, P. F. Bedaque, A. Parreno, and M. J. Savage, Nucl. Phys. **A747**, 55 (2005).
[46] R. A. Briceño, Z. Davoudi, T. C. Luu, and M. J. Savage, Phys. Rev. D **88**, 114507 (2013).
[47] G. Meng, C. Miao, X. Du, and C. Liu, Int. J. Mod. Phys. A **19**, 4401 (2004).
[48] P. F. Bedaque and J.-W. Chen, Phys. Lett. B **616**, 208 (2005).
[49] P. F. Bedaque, Phys. Lett. B **593**, 82 (2004).
[50] G. M. de Divitiis, R. Petronzio, and N. Tantalo, Phys. Lett. B **595**, 408 (2004).
[51] C. T. Sachrajda and G. Villadoro, Phys. Lett. B **609**, 73 (2005).
[52] K. Polejaeva and A. Rusetsky, Eur. Phys. J. A **48**, 67 (2012).
[53] R. A. Briceño and Z. Davoudi, Phys. Rev. D **87**, 094507 (2013).
[54] M. T. Hansen and S. R. Sharpe, Phys. Rev. D **90**, 116003 (2014).
[55] M. T. Hansen and S. R. Sharpe, Phys. Rev. D **92**, 114509 (2015).
[56] R. A. Briceño, M. T. Hansen, and S. R. Sharpe, Phys. Rev. D **95**, 074510 (2017).
[57] H. W. Hammer, J. Y. Pang, and A. Rusetsky, J. High Energy Phys. 10 (2017) 115.
[58] H.-W. Hammer, J.-Y. Pang, and A. Rusetsky, J. High Energy Phys. 09 (2017) 109.
[59] M. T. Hansen, H. B. Meyer, and D. Robaina, Phys. Rev. D **96**, 094513 (2017).
[60] M. Mai and M. Döring, Eur. Phys. J. A **53**, 240 (2017).
[61] M. Döring, H.-W. Hammer, M. Mai, J.-Y. Pang, A. Rusetsky, and J. Wu, Phys. Rev. D **97**, 114508 (2018).
[62] P. Guo, M. Döring, and A. P. Szczepaniak, Phys. Rev. D **98**, 094502 (2018).
[63] M. Mai and M. Döring, Phys. Rev. Lett. **122**, 062503 (2019).
[64] Y. Meng, C. Liu, U.-G. Meißner, and A. Rusetsky, Phys. Rev. D **98**, 014508 (2018).
[65] J. Bulava and M. T. Hansen, Phys. Rev. D **100**, 034521 (2019).
[66] M. T. Hansen and S. R. Sharpe, Annu. Rev. Nucl. Part. Sci. **69**, 65 (2019).
[67] A. W. Jackura, S. M. Dawid, C. Fernández-Ramírez, V. Mathieu, M. Mikhasenko, A. Pilloni, S. R. Sharpe, and A. P. Szczepaniak, Phys. Rev. D **100**, 034508 (2019).
[68] J.-Y. Pang, J.-J. Wu, H.-W. Hammer, U.-G. Meißner, and A. Rusetsky, Phys. Rev. D **99**, 074513 (2019).
[69] F. Romero-López, S. R. Sharpe, T. D. Blanton, R. A. Briceño, and M. T. Hansen, J. High Energy Phys. 10 (2019) 007.
[70] T. D. Blanton, F. Romero-López, and S. R. Sharpe, Phys. Rev. Lett. **124**, 032001 (2020).
[71] M. T. Hansen, R. A. Briceño, R. G. Edwards, C. E. Thomas, and D. J. Wilson (Hadron Spectrum Collaboration), Phys. Rev. Lett. **126**, 012001 (2021).
[72] C. Körber, E. Berkowitz, and T. Luu, arXiv:1912.04425.
[73] D. B. Leinweber, R. M. Woloshyn, and T. Draper, Phys. Rev. D **43**, 1659 (1991).
[74] D. J. Wilson, R. A. Briceño, J. J. Dudek, R. G. Edwards, and C. E. Thomas (Hadron Spectrum Collaboration), Phys. Rev. D **92**, 094502 (2015).
[75] R. A. Briceno, J. J. Dudek, R. G. Edwards, and D. J. Wilson, Phys. Rev. Lett. **118**, 022002 (2017).
[76] R. A. Briceño, J. J. Dudek, R. G. Edwards, and D. J. Wilson (Hadron Spectrum Collaboration), Phys. Rev. D **97**, 054513 (2018).
[77] V. Bernard, M. Lage, U.-G. Meißner, and A. Rusetsky, J. High Energy Phys. 08 (**2008**) 024.